Miner Deposita
DOI 10.1007/s00126-008-0228-9

ARTICLE

Examining potential genetic links between Jurassic porphyry Cu–Au±Mo and epithermal Au±Ag mineralization in the Toodoggone district of North-Central British Columbia, Canada

Paul Duuring · Stephen M. Rowins · Bradley S. M. McKinley · Jenni M. Dickinson · Larry J. Diakow · Young-Seog Kim · Robert A. Creaser

Received: 29 April 2008 / Accepted: 1 December 2008

Abstract The Toodoggone district comprises Upper Triassic to Lower Jurassic Hazelton Group Toodoggone Formation volcanic and sedimentary rocks, which unconformably overlie submarine island-arc volcanic and sedimentary rocks of the Lower Permian Asitka Group and Middle Triassic Takla Group, some of which are intruded by Upper Triassic to Lower Jurassic plutons and dikes of the Black Lake suite. Although plutonism occurred episodically from ca. 218 to 191 Ma, the largest porphyry Cu–Au±Mo systems formed from ca. 202 to 197 Ma, with minor mineralization occurring from ca. 197 to 194 Ma. Porphyry-style mineralization is hosted by small-volume (<1 km^3), single-phase, porphyritic igneous stocks or dikes that have high-K calc-alkaline compositions and are comparable with volcanic-arc granites. The Fin porphyry Cu–Au–Mo deposit is anomalous in that it is 16 m.y. older than any other porphyry Cu–Au±Mo occurrence in the district and has lower REEs. All porphyry systems are spatially restricted to exposed Asitka and Takla Group basement rocks, and rarely, the lowest member of the Hazelton Group (i.e., the ca. 201 Ma Duncan Member). The basement rocks to intrusions are best exposed in the southern half of the district, where high rates of erosion and uplift have resulted in their preferential exposure. In contrast, low- and high-sulfidation epithermal systems are more numerous in the northern half of the district, where the overlying Hazelton Group rocks dominate exposures. Cogenetic porphyry systems might also exist in the northern areas; however, if they are present, they are likely to be buried deeply beneath Hazelton Group rocks. High-sulfidation epithermal systems formed at ca. 201 to 182 Ma, whereas low-sulfidation systems were active at ca. 192 to 162 Ma. Amongst the studied epithermal systems, the Baker low-sulfidation epithermal deposit displays the strongest demonstrable genetic link with magmatic fluids; fluid inclusion studies demonstrate that its ore fluids were hot (>468°C), saline, and deposited metals at deep crustal depths (>2 km). Sulfur, C, O, and Pb isotope data confirm the involvement of a magmatic fluid, but also suggest that the ore fluid interacted with Asitka and Takla Group country rocks prior to metal deposition. In contrast, in the Shasta, Lawyers, and Griz-Sickle low-sulfidation epithermal systems, there is no clear association

Editorial handling: T. Bissig

P. Duuring (✉) · S. M. Rowins · B. S. M. McKinley · J. M. Dickinson
Department of Earth and Ocean Sciences,
University of British Columbia,
Vancouver, BC, Canada V6T 1Z4
e-mail: pduuring@hotmail.com

L. J. Diakow
British Columbia Geological Survey, Ministry of Energy,
Mines and Petroleum Resources,
Victoria, BC, Canada V8V 1X4

Y.-S. Kim
Department of Environmental Geosciences,
Pukyong National University,
608-737 Busan, South Korea

R. A. Creaser
Department of Earth and Atmospheric Sciences,
University of Alberta,
Edmonton, AB, Canada T6G 2E3

Present address:
P. Duuring
Department of Environmental Geosciences,
Pukyong National University,
608-737 Busan, South Korea

Published online: 16 January 2009

with magmatic fluids. Instead, their fluid inclusion data indicate the involvement of low-temperature (175 to 335°C), low-salinity (1 to 11 equiv. wt.% NaCl) fluids that deposited metals at shallow depths (<850 m). Their isotope (i.e., O, H, Pb) data suggest interaction between meteoric and/or metamorphic ore fluids with basement country rocks.

Keywords Porphyry · Epithermal · Toodoggone · Stikine · Kemess South · Kemess North

Introduction

Porphyry Cu–Au±Mo and epithermal Au±Ag deposits in magmatic arcs are commonly hosted by coeval calc-alkaline volcanic rocks and subvolcanic intrusive equivalents that form as a result of plate convergence and subduction (Sawkins 1990; Sillitoe and Hedenquist 2003). A consequence of their shared tectonic histories is that these deposits are frequently located in the same district and are approximately the same age (e.g., Mankayan district, Philippines—Arribas et al. 1995; Claveria 2001; Cooke and Bloom 1990; Hedenquist et al. 1998; Sajona et al. 2002). The Toodoggone district in British Columbia, Canada is a 100-km-long by 30-km-wide NNW-trending belt of island-arc volcano plutonic rocks located along the ENE margin of the Stikine terrane. Within the district, several proximal porphyry and epithermal deposits have mineralization ages that are broadly coeval with Jurassic calc-alkaline plutonism and volcanism (Diakow et al. 1991). Despite their spatial and timing relationships, a genetic link between the porphyry and epithermal systems is equivocal because of the lack of a systematic comparison between key deposits in the district.

This study evaluates the possible genetic link between porphyry and epithermal systems in the Toodoggone district by integrating district-scale geological mapping and geochronological studies (e.g., Diakow 2001; Diakow et al. 1991, 1993) with detailed deposit models for key porphyry and epithermal deposits in the district. Such detailed deposit models exist for the Kemess South (Duuring et al. 2008), Kemess North (McKinley 2006), and Pine–Fin–Mex (Dickinson 2006) porphyry Cu–Au–Mo systems and the Shasta (Thiersch et al. 1997) low-sulfidation epithermal Ag–Au system. This paper presents geological summaries for each major porphyry and epithermal occurrence in the district, interprets likely source areas for metals and fluids based on fluid inclusion studies and S, C, O, and Pb isotope data for mineralized veins, and comments on the association between porphyry and epithermal systems in the district.

Methodology

Detailed lithological and structural mapping of surface and pit exposures at 1:500 to 1:5,000 scales was performed at the Kemess South, Kemess North, Pine–Fin–Mex, and Sofia porphyry Cu–Au±Mo occurrences and the Shasta, Baker, Lawyers, and Griz-Sickle epithermal occurrences. Structural orientations are generally given as dip angle/strike directions or plunge/trend orientations, with reference to True North. Unless otherwise indicated for strikes, right-hand rule is observed.

Hand specimens of least-altered rocks were collected from outcrop, pit exposures, and diamond drill core for thin-section petrography and geochemical analysis. Representative, least-altered, drill core samples (0.5 to 1 kg) were used for whole-rock major and trace element analysis. The samples were photographed, cleaned, and reduced to a powder using an agate crusher and mill. Major elements were determined by X-ray fluorescence, whereas trace element analyses were measured by inductively coupled plasma-mass spectrometry at ALS Chemex, Vancouver. Hand specimens of least-altered rocks and hypogene alteration assemblages adjacent to veins were etched by hydrofluoric acid and stained by sodium cobaltinitrite to aid in the identification of feldspars and estimation of mineral proportions.

Sulfide and sulfate minerals were hand picked from crushed unweathered vein and altered rock samples for sulfur isotope studies. Sulfur isotope analyses were undertaken at the G.G. Hatch Isotope Laboratories, University of Ottawa, Canada using the same techniques described by Duuring et al. (2008). Calcite was hand picked from crushed vein and rock samples and submitted for carbon and oxygen stable isotope analysis at the G.G. Hatch Isotope Laboratories, University of Ottawa, Canada. The $\delta^{13}C$ and $\delta^{18}O$ values were determined using a Delta XP and a Gas Bench II following the methods of Coplen et al. (1983) and Al-Aasm et al. (1990). Sulfide minerals, feldspars, and calcite were hand picked from crushed vein and rock samples and submitted for radiogenic lead isotope analysis at the PCIGR at the University of British Columbia, Canada. For pyrite separates, 10 to 50 mg of each sample was leached in dilute hydrochloric acid to remove surface contamination before dissolution in nitric acid. For feldspar separates, 10 to 50 mg of each sample was leached in dilute hydrochloric acid, followed by washing in dilute hydrofluoric/hydrobromic acids to remove surface contamination, before dissolution in hydrofluoric acid. Ion-exchange column techniques were used to separate and purify lead. The samples were converted to bromide, the solution was passed through ion exchange columns in hydrobromic acid, and the lead eluted in 6 N hydrochloric acid. Approximately 10 to 25 ng of the lead in

chloride form was loaded on Re filaments using a phosphoric acid–silica gel emitter, and isotopic compositions were determined in peak-switching mode using a modified VG54R thermal ionization mass spectrometer. The measured ratios were corrected for instrumental mass fractionation of 0.12% (Faraday collector) per mass unit based on repeated measurements of the N.B.S. SRM 981 Standard Isotopic Reference Material and the values recommended by Thirlwall (2000). Errors were numerically propagated, including all mass fractionation and analytical errors, using the technique of Roddick (1987). The total procedural blank on the trace lead chemistry was 110 pg.

Regional geology

Key relationships between rock types, metamorphism, and structures in the Toodoggone district are described in detail by Duuring et al. (2008); only a brief summary of these features are included here. The oldest known basement rocks in the district are submarine island-arc rhyolitic and basaltic volcanic rocks, siltstone, and limestone of the Lower Permian Asitka Group (ca. 308 Ma; Diakow 2001). These rocks are unconformably overlain by basaltic lava, with interbedded lapilli tuff and volcanic breccia units of the Middle Triassic Takla Group (ca. 216 Ma; Monger and Church 1977). Asitka and Takla Group rocks are mostly fault bounded and most are exposed in the southern half of the district, adjacent to exposed plutons (Fig. 1). The basement rocks are unconformably overlain by Upper Triassic to Lower Jurassic Hazelton Group volcanic and sedimentary rocks (Diakow et al. 1991, 1993). Toodoggone Formation rocks of the Hazelton Group underlie most of the northern half of the district. Only the lower members of the Toodoggone Formation are exposed with Asitka and Takla Group basement rocks in southernmost areas (Fig. 1). Lower to Upper Cretaceous continental clastic rocks of the Sustut

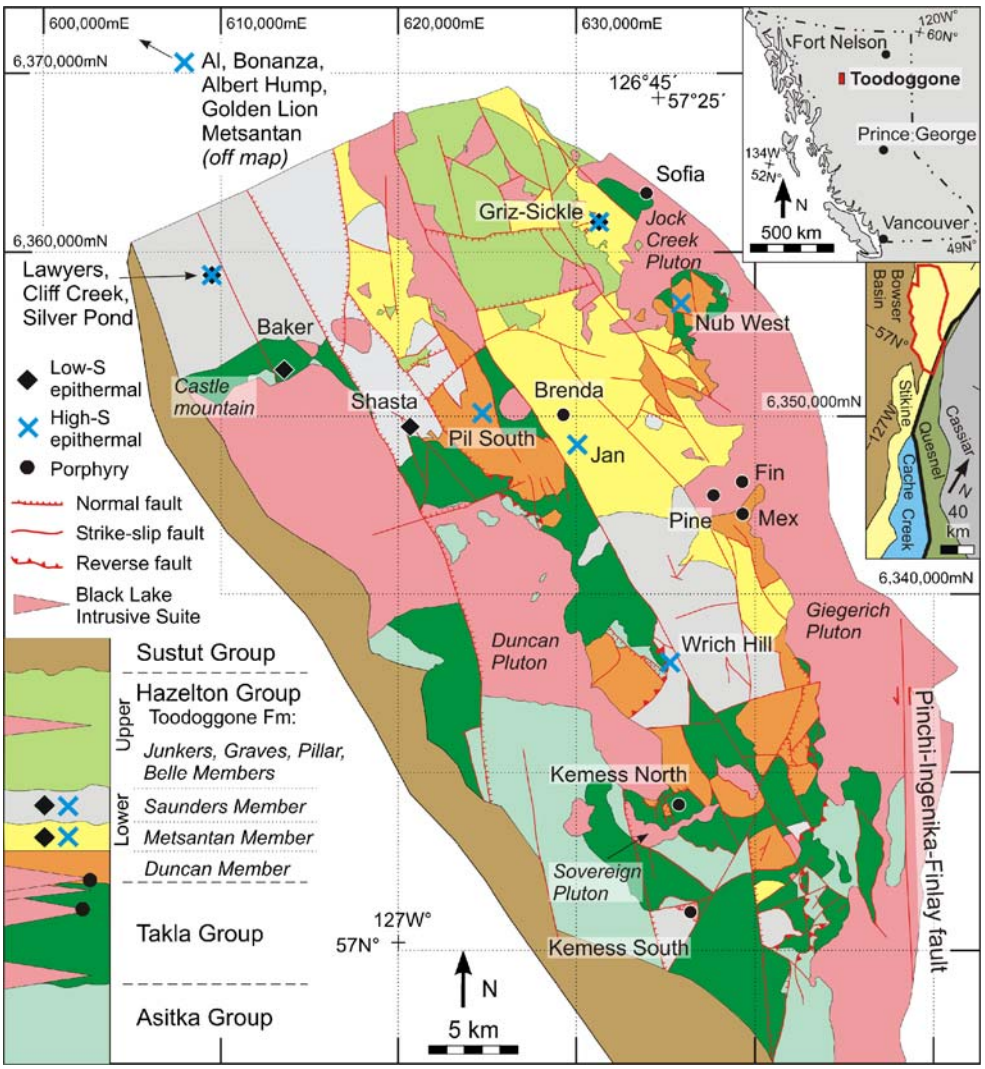

Fig. 1 The simplified geology map of the southern half of the Toodoggone district, south of the Toodoggone river, shows the distribution of rock types, structures, and porphyry Cu–Au–Mo and epithermal Au±Ag occurrences. The geological interpretation is based on regional mapping reported by Diakow (2001, 2004, 2006a) and Diakow et al. (2005). The two *inset maps* show the location of the Toodoggone district in British Columbia and the relationship between the district and recognized terranes in British Columbia (the outline of the southern Toodoggone district is defined by a *thick red line*, whereas the Pinchi–Ingenika–Finlay fault that separates the Stikine and Quesnel terranes is delineated by a *thick black line*)

Group overlap the western margin of the Toodoggone district (Fig. 1). Asitka, Takla, and Hazelton Group volcano-sedimentary rocks are intruded by Upper Triassic to Lower Jurassic felsic to intermediate plutons and cogenetic dikes of the Black Lake suite (Diakow 2001, 2006b; Diakow et al. 1993; Mortensen et al. 1995). The plutons are exposed along the margins of the Toodoggone volcanic-sedimentary depression but also occur internally within the depression as elongate, NW- to NE-trending plutons (Fig. 1). Up to zeolite-facies regional metamorphism affects Toodoggone Formation rocks, whereas underlying Takla Group rocks experienced prehnite–pumpellyite metamorphism (Diakow et al. 1993). High-temperature contact metamorphism is locally associated with plutonic rocks and dikes. Consequently, the prefix "meta" is implied but omitted from lithological descriptions that follow.

Porphyry Cu–Au±Mo systems

Kemess South

Kemess South is the only Cu–Au–Mo mine in the district and a major Cu and Au producer in British Columbia. Kemess South has a past production to 31 Dec. 2007 of 161 Mt containing 0.71 g/t Au and 0.23% Cu, and proven plus probable reserves of 51.8 Mt containing 0.47 g/t Au and 0.17% Cu (Skrecky, unpublished report for Northgate Minerals Corp., 2008). Relationships between lithologies, structures, veins, and alteration are described by Duuring et al. (2008). In summary, Cu–Au–Mo mineralization is mainly hosted by the 199.6±0.6 Ma (2σ) (Mortensen et al. 1995) Maple Leaf granodiorite, which intrudes folded, Permian Asitka Group siltstone and limestone, and massive Triassic Takla Group basalt. Southwest-dipping, 194.0±0.4 Ma (Diakow 2001) Toodoggone Formation conglomerate, volcaniclastic, and epiclastic rocks unconformably overlie the granodiorite and Asitka Group rocks. Granodiorite displays an intrusive contact with mineralized and altered Takla Group basalt but a sheared contact with unmineralized and less altered Asitka Group siltstone. Low-tonnage, high-grade, remobilized Cu zones occur beneath a 30-m-thick leached capping in supergene-altered granodiorite and in exotic positions in overlying Toodoggone Formation rocks. Mineralization related to stage 3 veins at Kemess South (main stage ore) is dated at 201.1±1.2 and 201.3±1.2 Ma by Re–Os dating of molybdenite (Duuring et al. 2008).

Kemess North

Kemess North lies 7 km north of Kemess South (Fig. 1) and has a proven plus probable reserve of 424 Mt containing 0.30 g/t Au and 0.16% Cu (Gray et al., unpublished report for Northgate Minerals Corp., 2005). Porphyry-style Cu–Au–Mo mineralization is mainly hosted by a ca. 202 Ma (Diakow 2006b), moderately SE-plunging diorite and overlying Takla Group basalt country rock. The diorite is presently overlain by about 500 m of Cu–Au–Mo-bearing Takla Group basalt country rock that is intensely weathered and locally gossanous. The 202.7±1.9 Ma (Diakow 2001) Sovereign diorite intrudes basalt about 1 km to the south of the Kemess North diorite. Both plutons have comparable emplacement ages, igneous mineral assemblages, and chemistries (Appendix 1); however, where tested, the Sovereign diorite is unmineralized and their genetic relationship is unclear. Toodoggone Formation volcaniclastic rocks that have a maximum depositional age of 199.1±0.3 Ma (Diakow 2001) crop out as prominent N-trending ridges or in isolated, down-faulted grabens within Takla Group basalt. Immediately NW of the deposit, the 197.3±1.1/0.9 Ma (Diakow 2001) Duncan diorite intrudes Takla Group basalt and Toodoggone Formation rocks, and is unmineralized.

Early-stage veins include magnetite stringer veins and quartz–magnetite–pyrite±chalcopyrite±molybdenite veins. These veins are restricted mainly to the Kemess North diorite, are locally associated with biotite±alkali feldspar (i.e., potassic) alteration, and are responsible for most of the Cu–Au–Mo mineralization at Kemess North. Main-stage quartz–pyrite±chalcopyrite±molybdenite veins are the most abundant vein type and are hosted by the diorite and proximal Takla Group basalts. The veins are associated with sericite–quartz–pyrite (i.e., phyllic) alteration and have a Re–Os molybdenite age of 201.8±1.2 Ma (McKinley 2006). Late-stage pyrite–chalcopyrite and anhydrite±pyrite±chalcopyrite veins and associated sericite–quartz–pyrite or chlorite–pyrite–illite (i.e., intermediate argillic) alteration occur in the diorite and Takla Group country rocks. Post-mineralization-stage anhydrite and carbonate–zeolite veins cut all rocks. An E–W-striking, steeply S-dipping fault truncates the northern extremity of the ore body and structurally juxtaposes mineralized diorite and Takla Group basalt country rock against poorly mineralized Toodoggone Formation rocks. The E–W striking fault is in turn cut by NW- to NE-striking faults, resulting in vertical graben-and-horst block displacements throughout the deposit. Remobilized Au and Cu are locally present within NW-trending fault zones that cut Takla Group basalt and Toodoggone Formation rocks in areas within approximately 100 m of the diorite-hosted ore body.

Fluid inclusion studies indicate that early- and main-stage ore fluids deposited Cu–Au–Mo at about 375 to 400°C and at crustal depths of >3 km (McKinley 2006). Sulfur and Pb isotope data suggest that metals in the early-stage ore fluid were mainly derived from the same magmatic chamber as

the Kemess North diorite, whereas main-stage veins record interaction between magmatic-derived fluids and Takla Group country rock prior to metal deposition. Carbon and O isotope data indicate that post-mineralization-stage calcite–zeolite veins formed from meteoric and/or metamorphic fluids (McKinley 2006).

Fin, Pine, and Mex

The Fin, Pine, and Mex porphyry Cu–Au±Mo systems are located within 2 km of each other in the central part of the study area (Fig. 1). At least two separate episodes of plutonism are responsible for mineralization in the area (Dickinson 2006).

The Fin monzogranite is the oldest dated pluton in the district, with a U–Pb zircon emplacement age of 217.8±0.6 Ma (Dickinson 2006). Two main-stage gold-bearing quartz–pyrite–chalcopyrite±molybdenite±sphalerite veins that cut the monzogranite give anomalously older Re–Os molybdenite mineralization ages of 221.0±1.4 Ma and 220.4±1.4 Ma (Dickinson 2006), suggesting that these veins cut a slightly older, undated magmatic phase. Main-stage veins are surrounded by pervasive epidote and chlorite alteration. Copper, Mo, and Ag concentrations are positively correlated with each other in the Fin monzogranite, whereas Pb correlates closely with Zn (Appendix 1). Late-stage pyrite±chalcopyrite and molybdenite±sphalerite± pyrite veins are cut by post-mineralization-stage epidote± chlorite, zeolite, and anhydrite–gypsum veins. Lead isotope values for sulfide minerals from the main-stage veins suggest that magmatic-derived fluids interacted with country rocks and possibly meteoric or metamorphic fluids before mineralization.

The Pine porphyry system (proven reserve of 40 Mt of ore containing 0.57 g/t Au and 0.15% Cu; Rebagliati et al. 1995) lies SW of the Fin porphyry system. The main host to porphyry-style Cu–Au–Mo mineralization is the Pine quartz monzonite, which has a U–Pb zircon emplacement age of 197.6±0.5 Ma (Dickinson 2006) and intrudes, alters, and locally mineralizes adjacent 200.9±0.4 Ma (Dickinson 2006) Duncan Member rocks of the Toodoggone Formation. The Pine quartz monzonite has a central potassic alteration zone that is flanked by phyllic and distal propylitic alteration zones in surrounding Toodoggone

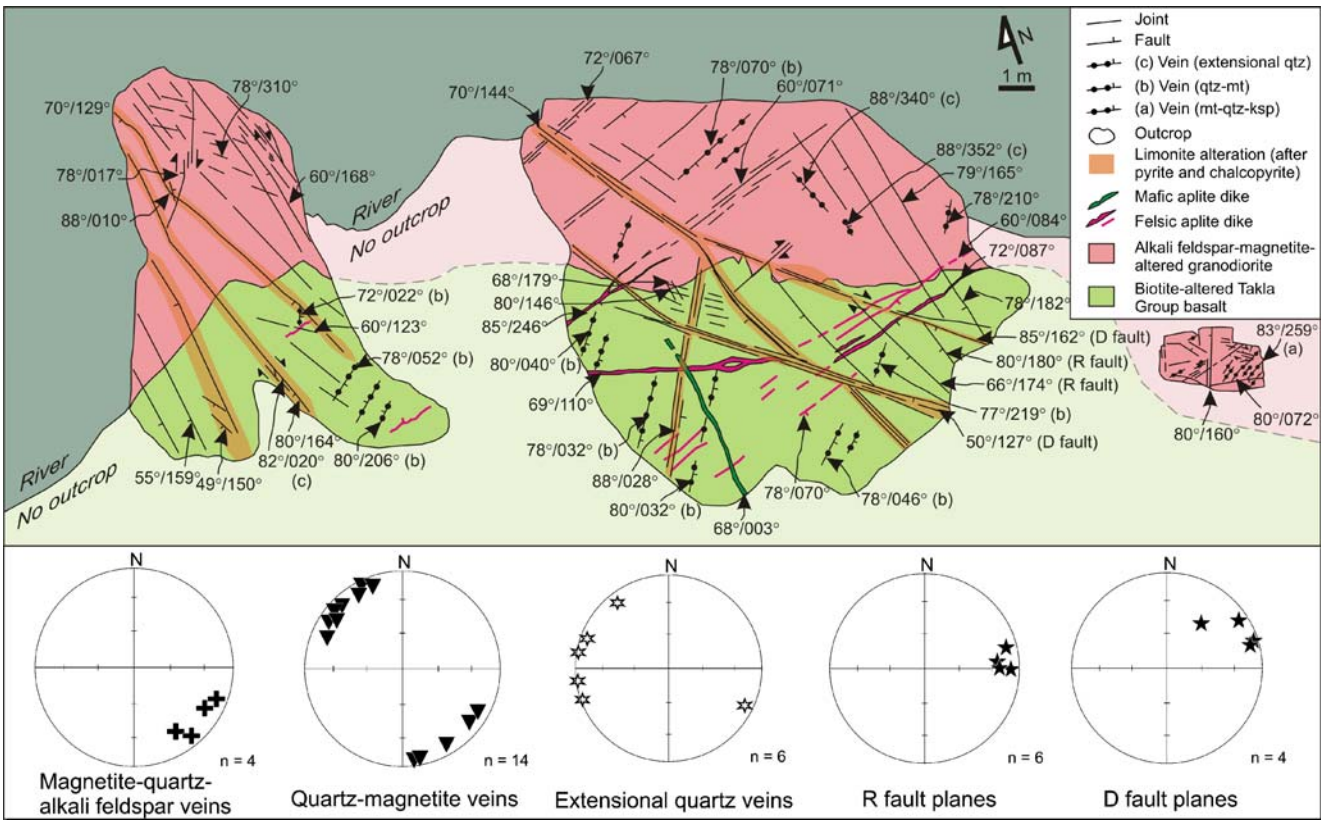

Fig. 2 The simplified geology map of the Sofia outcrop shows the intrusive contact between alkali feldspar–magnetite-altered Sofia granodiorite and biotite-altered Takla Group basalt. Hematite-altered felsic aplite dikes cut both rock types and are in turn cut by mafic aplite dikes. The dikes are cut by magnetite–quartz–alkali feldspar veins, quartz–magnetite veins, and extensional quartz veins. All lithologies and structures are cut by brittle, N- and NW-striking, steeply WSW-dipping R and D fault zones that host quartz–chlorite–pyrite–chalcopyrite–gold veins and chlorite alteration halos. The lower-hemisphere equal area stereoplots show the distribution of selected planar structures

Formation country rock. Main-stage Au–Cu±Mo mineralization is most intense in the Pine quartz monzonite and is genetically related to quartz–magnetite–chalcopyrite–pyrite veins, which are magnetite-rich and sulfide-poor, and surrounded by potassic (alkali feldspar–magnetite) alteration. Copper and Au concentrations display a positive correlation with Mo, Ag, Pb, and Zn. Main-stage veins and alteration minerals formed from a magmatic-derived, high-temperature (430 to 550°C) fluid (Dickinson 2006). Late-stage anhydrite–pyrite±specular hematite±chalcopyrite, quartz–pyrite±chalcopyrite, and pyrite±chalcopyrite veins and associated phyllic alteration zones formed in the Pine quartz monzonite at the same time as the nearby Pine granodiorite stock was emplaced (Dickinson 2006). Metals were initially deposited from the late-stage fluid at temperatures of 430 to 460°C, which fell to temperatures of about 340°C during the formation of later veins. Lead isotope values for sulfide minerals from late-stage veins indicate a metal contribution from a magmatic source as well as fluid interaction with Takla Group country rocks. The final mineralization phase of the Pine porphyry Cu–Au–Mo system is temporally constrained by the emplacement of weakly Cu-bearing syenite dikes (U–Pb zircon age of 193.8 ±0.5 Ma; Dickinson 2006), whereas the final stage of magmatism at Pine is defined by the emplacement of post-mineral rhyolite dikes (U–Pb zircon age of 193.6±0.4 Ma; Dickinson 2006).

The Mex porphyry Cu–Au±Mo system to the SE of Pine is poorly understood due to limited outcrop and drilling. The Mex monzonite is cut by quartz–magnetite–pyrite–

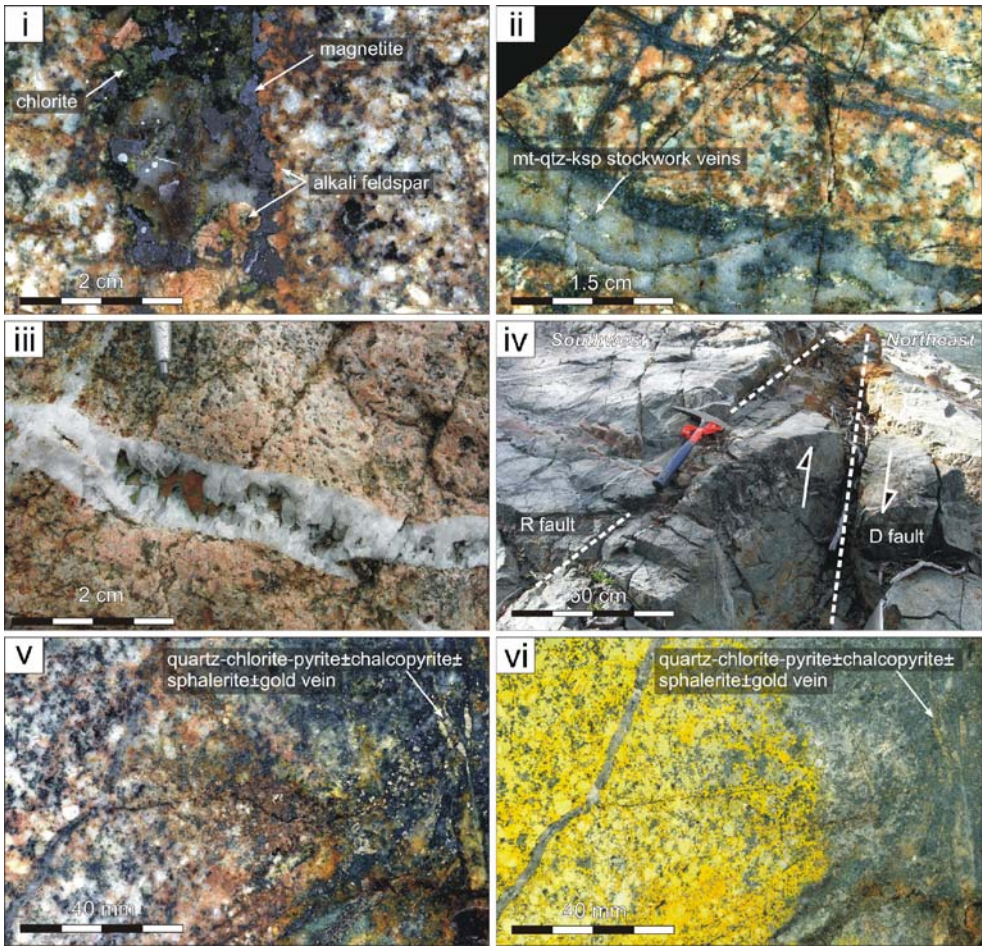

Fig. 3 Photographs of representative vein types at Sofia: *i* Alkali feldspar–magnetite-altered granodiorite is cut by a 2-cm-thick magnetite–quartz–alkali feldspar vein that has irregular margins rimmed by a <5-mm-thick halo of alkali feldspar and magnetite. Alkali feldspar is partly altered to epidote and chlorite, whereas magnetite is altered to hematite. *ii* Magnetite–quartz–alkali feldspar stockwork veins and <5-mm-thick alkali feldspar halos in granodiorite are cut by a 1-cm-thick banded quartz–magnetite vein. *iii* A 1-cm-thick extensional quartz vein with euhedral quartz crystals cuts alkali feldspar–magnetite–chlorite–epidote-altered granodiorite. *iv* Coeval R and D chlorite–quartz–pyrite–chalcopyrite–gold-altered fault zones cut the granodiorite and all vein types. The fault zones are supergene-altered to limonite and goethite. *v* Close up of a quartz–chlorite–pyrite ±chalcopyrite±sphalerite±gold vein associated with a R fault zone. Chlorite and pyrite replace alkali feldspar and magnetite alteration in the granodiorite. *vi* Staining with sodium cobaltinitrite demonstrates the replacement of alkali feldspar by chlorite with proximity to the vein. Abbreviations: *mt* magnetite, *qtz* quartz, *ksp* alkali feldspar

chalcopyrite veins with associated alkali feldspar–magnetite (potassic) alteration. Potassic alteration is surrounded by quartz–pyrite–sericite (phyllic) alteration and more distal chlorite–epidote (propylitic) alteration zones in the Mex monzonite. The magmatic–hydrothermal footprint of the Mex porphyry system is much smaller than the Pine system, possibly because it has been truncated by the Mex fault, which juxtaposes the Mex monzonite against unmineralized Giegerich granodiorite located to the S (Dickinson 2006).

Sofia

The Sofia prospect is located in a river valley about 5 km to the NE of the Griz-Sickle low- and high-sulfidation epithermal occurrences (Fig. 1). The prospect is mostly covered by >10-m-thick glacial till with minor outcrop occurring along river banks. No drill holes exist at the time of the study; hence, all geological relationships are based on a small 40 m^2 area of outcrop (Fig. 2). This outcrop exposes an E–W striking intrusive contact between alkali feldspar–magnetite-altered, porphyritic granodiorite and biotite–magnetite-altered, porphyritic Takla Group basalt country rock. Both rock types are cut by 1- to 10-cm-thick, E–W-striking, near-vertical, hematite-altered felsic aplite dikes, which are in turn cut by 5- to 10-cm-thick, N-striking, E-dipping mafic aplite dikes.

Granodiorite and basalt are cut by a series of 1- to 10-cm-thick, near-vertical, NE-trending veins that include rare magnetite–quartz–alkali feldspar±chalcopyrite veins (Fig. 3 i), numerous quartz–magnetite veins (Fig. 3 ii), and minor extensional quartz veins (Fig. 3 iii). The magnetite–quartz–alkali feldspar±chalcopyrite and quartz–magnetite veins are surrounded by <5-cm-thick pink alkali feldspar–magnetite alteration zones that coalesce to form pervasive potassic alteration in the granodiorite. These veins and their alteration halos also occur in basalt country rock, although hydrothermal biotite occurs instead of alkali

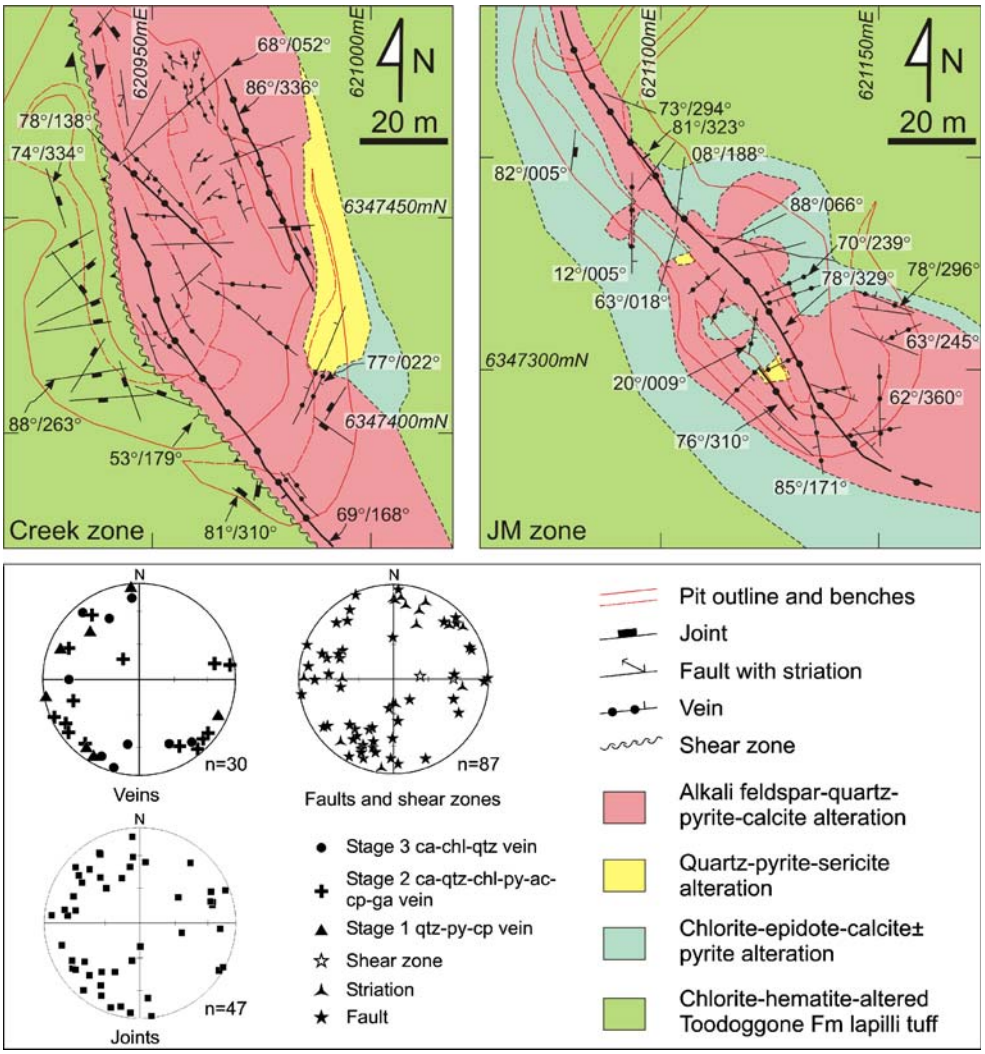

Fig. 4 Simplified geology maps of the Creek and JM Ag–Au orebodies at the Shasta low-sulfidation epithermal deposit. The maps of the two <30-m-deep pits (spaced 80 m apart along a NW trend) show the relative distribution of hypogene hydrothermal alteration and major structures. Both orebodies are characterized by several 1- to 2-m-thick, NW-striking mineralized veins that are surrounded by inner potassic, phyllic, and outer propylitic alteration zones that replace earlier chlorite–hematite-altered Toodoggone Formation lapilli tuffs. The lower-hemisphere equal area stereoplots show the distribution of selected planar and linear structures. Abbreviations: *ac* acanthite, *ca* calcite, *chl* chlorite, *cp* chalcopyrite, *ga* galena, *py* pyrite, *qtz* quartz

feldspar. Magnetite–quartz–alkali feldspar±chalcopyrite veins and quartz–magnetite veins are cut by felsic and mafic aplite dikes. These dikes are cut by extensional quartz veins that do not show obvious alteration halos in granodiorite and comprise <3-mm-long euhedral quartz grains that grow inwards from vein margins toward central vugs. Primary fluid inclusions are located in the cores of zoned quartz grains and include randomly distributed, negative crystal-shaped, two-phase, liquid-rich, aqueous fluid inclusions. All lithologies and vein types are cut by brittle, N- and NW-striking, steeply WSW-dipping R and D fault zones (terminology after Riedel 1929) that host <1-m-wide quartz–chlorite–pyrite±chalcopyrite±sphalerite±gold veins surrounded by chlorite–pyrite alteration (Fig. 3 iv to vi). These fault-hosted veins contain metal concentrations of up to 410 ppm Au and 1,230 ppm Cu, and are surrounded by chlorite–pyrite alteration halos that are weathered to limonite and goethite. The faults offset all earlier vein types with dextral displacements of up to 1 m.

After emplacement of the Sofia granodiorite, NE–SW-directed shortening resulted in formation of NE-striking magnetite–quartz–alkali feldspar±chalcopyrite and quartz–magnetite veins. A resumption in magmatism led to the generation of felsic and mafic aplite dikes, which cut earlier veins. Later N–S-directed shortening within a brittle–ductile deformation regime resulted in N-striking, extensional quartz veins that lack alteration envelopes. Continued N–S-directed shortening produced the dextral

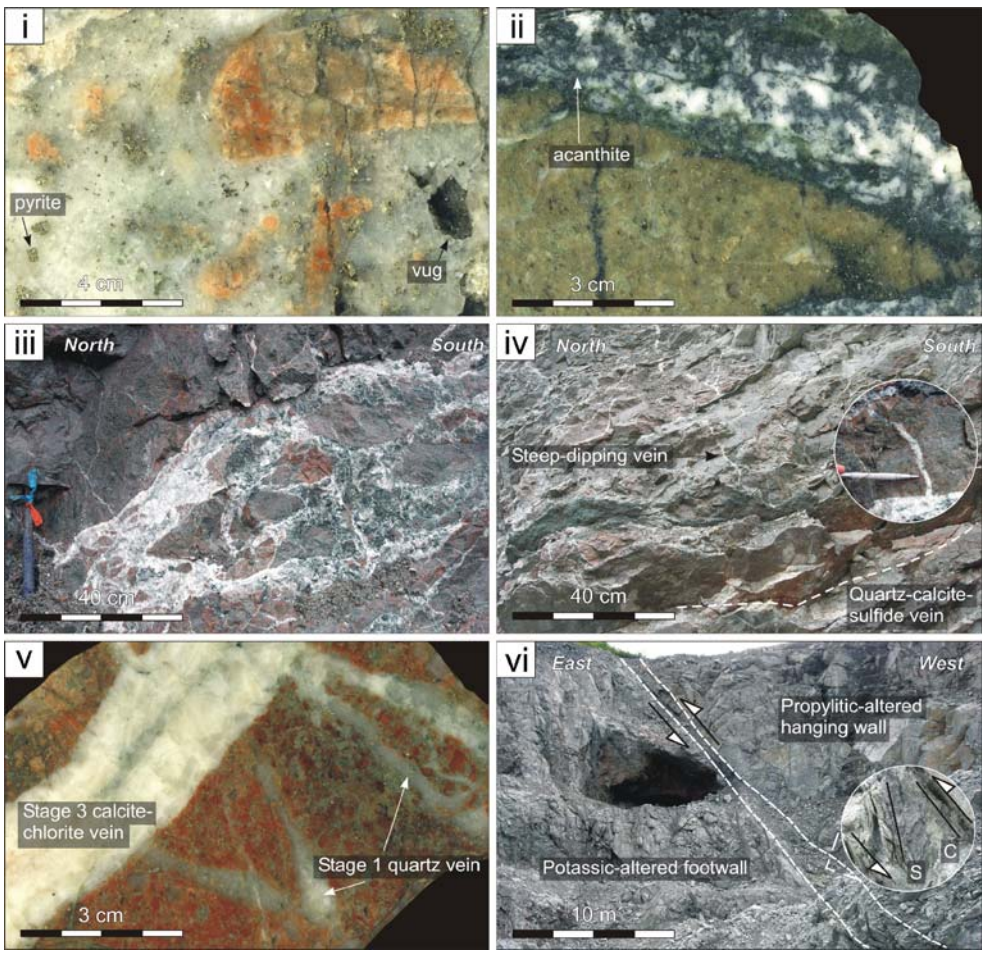

Fig. 5 Photographs of representative vein types at Shasta: *i* A 10-cm-thick stage 1 quartz–pyrite–chalcopyrite hydrothermal breccia vein hosts disseminated pyrite that locally rims angular fragments of alkali feldspar-altered lapilli tuff wallrock. The 1-cm-diameter vug has euhedral quartz crystals growing towards the center of the vug. *ii* Quartz–sericite–pyrite-altered lapilli tuff is cut by a stage 2 calcite–chlorite–acanthite–pyrite–galena–sphalerite–chalcopyrite vein. *iii* A 60-cm-thick zone of calcite–quartz–chlorite hydrothermal breccia cuts alkali feldspar-altered lapilli tuff in the E wall of the Creek zone pit. Coeval calcite–quartz–chlorite stockwork veins propagate away from the breccia zone. *iv* Steep-dipping stage 2 calcite–quartz–chlorite veins stem from larger NW-tending calcite–quartz–chlorite veins in the E wall of the JM zone pit. *v* A coarse-grained, stage 3 calcite–chlorite vein cuts alkali feldspar-altered lapilli tuff and stage 1 quartz±pyrite veins. *vi* A late, <1-m-thick, SE-striking, SW-dipping reverse-sinistral shear zone truncates the Creek zone ore body and juxtaposes alkali feldspar-altered, quartz vein-rich tuff against chlorite-altered tuff. The *inset* shows a photographic enlargement of the shear zone; S–C shear fabric relationships indicate reverse displacement (the enlargement shows a 3-cm-diameter region of the shear zone)

R and D fault zones that contain quartz–chlorite–pyrite± chalcopyrite±sphalerite±gold veins and have associated Cu–Au–Zn mineralization.

Epithermal Au±Ag systems

Low-sulfidation systems

Shasta

The Shasta deposit, previously known as the Shas deposit, has combined original reserves of 1.6 Mt of ore containing 2.84 g/t Au and 132.2 g/t Ag (Thiersch et al. 1997). The deposit includes the Creek and JM zone orebodies, which are up to 1 km long, 20 m wide, and extend to vertical depths of 300 m (Thiersch et al. 1997). The Creek zone is exposed in the hillside about 50 m below the JM zone. Previous studies at Shasta have focused on stratigraphic and structural relationships in the near-deposit environment (Marsden and Moore 1990) as well as hydrothermal fluid processes controlling Ag–Au mineralization in the Shasta deposit (Thiersch et al. 1997). Work completed by this study includes 1:250-scale structural and hydrothermal alteration mapping of new exposures in the two pits that overlie the Creek and JM zones (Fig. 4). Samples were collected for fluid inclusion and isotope analyses.

Least-altered country rock at Shasta includes a coarse-grained, chlorite±hematite±epidote±calcite (i.e., propylitic)- altered Toodoggone Formation dacitic lapilli tuff. The propylitic alteration is widespread and locally replaced by alteration minerals associated with the Shasta Au–Ag veins. Hence, propylitic alteration is probably the result of an early regional-scale event that pre-dates Au–Ag mineralization (Marsden and Moore 1990; Thiersch et al. 1997). Proximal hydrothermal alteration zones associated with the Creek and JM zone orebodies are <50 m thick, NW-trending, and contain alkali feldspar, quartz, pyrite, and calcite (Fig. 4). These potassic alteration zones are locally replaced by <20-m-thick quartz–sericite–pyrite (i.e., phyllic) alteration zones. Chlorite–epidote–calcite±pyrite (i.e., propylitic) alteration zones that are <30-m-thick flank potassic and phyllic alteration zones and decrease in intensity away from the orebodies.

Earliest-forming veins in the Shasta deposit are stage 1 quartz–pyrite–chalcopyrite±galena±sphalerite veins. They are mostly steep dipping but display variable strike orientations (Fig. 4). Stage 1 veins commonly contain vugs and angular fragments of intensely alkali feldspar–quartz–pyrite-altered wallrock that are rimmed by microcrystalline quartz (Fig. 5 i). Alkali feldspar in hydrothermal alteration zones surrounding these veins returned an Ar–Ar age of 186.7±1.7 Ma for the potassic hydrothermal alteration event (Clark and Williams-Jones 1991). Stage 1 veins are cut by <1-m-thick, steep-dipping (80°), NW- and SW-striking, stage 2 calcite–chlorite–acanthite–pyrite–galena–sphalerite–chalcopyrite±silver±electrum veins and zones of hydrothermal breccia that are surrounded by calcite–chlorite±sericite alteration zones (Fig. 5 ii and iii). Locally, <2-cm-thick and <3-m-long calcite–chlorite–pyrite–acanthite ladder veins branch at right angles from larger hydrothermal breccia zones (Fig. 5 iv). Stage 3 calcite–chlorite veins cut all other vein types and alteration styles (Fig. 5 v), are <50 cm thick, and display <1-cm-long euhedral calcite crystals growing from vein margins. These veins are steep dipping (60° to 90°) and strike NE or WNW (Fig. 4).

Brittle–ductile faults cut and offset stage 1, 2, and 3 veins. The faults display a wide range of orientations but most are steep dipping (50° to 90°) and strike to the WNW or NNE (Fig. 4). A >150-m-long, <1-m-thick, SSE-striking, moderately WSW-dipping shear zone (referred to as the Shasta fault by Marsden and Moore 1990) cuts the Creek zone veins and ore body, and structurally juxtaposes potassic- and propylitic-altered lapilli tuff (Fig. 5 vi). The shear zone displays S and C shear fabrics and slickenslides that pitch about 70° to the S, and indicate reverse-dextral movement. Joints throughout the Shasta deposit display the same structural trends as brittle–ductile faults (Fig. 4). Marsden and Moore (1990) interpret NW- and SW-striking veins to be conjugate sets that formed as a result of N–S directed shortening. Later veins and faults probably formed during reactivation of these structures.

Microthermometry was performed on two stage 2 calcite–chlorite–acanthite–pyrite–galena–sphalerite–chalcopyrite± silver±electrum veins collected from the Creek and JM zones (Fig. 6 i). Stage 2 quartz, calcite, galena, sphalerite, chalcopyrite, acanthite, silver, and gold are cogenetic (Fig. 6 ii). Translucent sphalerite commonly hosts two-phase (liquid–vapor) aqueous primary fluid inclusions that are elongate to equant, negative crystal-shaped, and occur along crystal growth zones in sphalerite (Fig. 6 iii). Pseudosecondary fluid inclusions in sphalerite have a similar morphology and composition to the primary inclusions but occur as trails that terminate at sphalerite grain boundaries. Undeformed, multiply twinned calcite grains that are rimmed by sphalerite and galena also host primary and pseudosecondary fluid inclusions. The fluid inclusions in calcite have the same composition as the inclusions hosted by sphalerite but are more equant (Fig. 6 iv). Microthermometry data for fluid inclusion assemblages (FIAs) measured from the Creek and JM zones are presented in Appendix 2 and are shown graphically in Fig. 7; the data ranges suggest that there are negligible differences in fluid properties between the Creek and JM zone orebodies. For both orebodies,

measured inclusions are 3 to 20 μm long (mean=7±4 μm, 1σ, n=51) and 2 to 20 μm wide (mean=4±3 μm, n=51). Eutectic temperatures (T_e) for primary and pseudosecondary inclusions range from −33.0 to −23.0°C, whereas final ice melting temperatures (T_m) range from −3.0 to −0.6 (mean=−2.0±0.6°C, n=29). No CO_2 was detected in any fluid inclusion. The T_e are below the eutectic temperature for the H_2O–NaCl system (i.e., −20.8°C) and indicates the presence of dissolved salts other than NaCl (Shepherd et al. 1985). Final ice melting temperatures correspond to calculated salinities of 1.0 to 4.9 equiv. wt.% NaCl (mean=3.1±1.0 equiv. wt.% NaCl, n=29). The inclusions homogenize to the liquid phase at temperatures that range from 231 to 303°C (mean=261±24°C, n=49). These salinity and total homogenization temperature ranges correspond closely to those reported by Thiersch et al. (1997) (i.e., 0 to 4 equiv. wt.% NaCl and 225 to 280°C). The Thiersch et al. (1997) study also documents the presence of coeval vapor-rich and liquid-rich aqueous primary fluid inclusions that are interpreted by these researchers to represent evidence of boiling during vein formation. They invoke fluid boiling during hydrothermal brecciation to cause removal of H_2S from the fluid, a corresponding increase in pH and fO_2, and probably a decrease in the liquid temperature, which led to the destabilization of bisulfide complexes and metal deposition. Assuming that the hydrothermal fluid was boiling at the time of stage 2 metal deposition, the total homogenization temperatures represent true trapping temperatures. Trapping pressures from the Thiersch et al. (1997) study are about 64 bar, which is equivalent to lithostatic depths of about 295 m, or hydrostatic depths of about 775 m.

Thiersch et al. (1997) report country rock pyrite $\delta^{34}S$ values that range from −0.7‰ to −2.5‰, vein pyrite $\delta^{34}S$ values range from −3.4‰ to −5.7‰, and two composite samples of sphalerite, galena, and acanthite have $\delta^{34}S$ values of −5.4‰ and −7.3‰ (Thiersch et al. 1997). Oxygen isotope data for hydrothermal quartz and calcite in equilibrium with a hydrothermal fluid at 280°C have $\delta^{18}O_{fluid}$ values of −1.5‰ to −4.1‰, whereas δD_{fluid} values for quartz are −148‰ to −171‰ (Thiersch et al. 1997). The O, H, and S isotope values suggest that the ore fluid had a meteoric origin but interacted with volcanic wallrocks and possibly gained S from nearby degassing magmas prior to ore deposition (Thiersch et al. 1997).

Baker

The Baker deposit, formerly known as Chappelle, includes at least seven Au–Ag–Cu-bearing quartz veins that occur within 4 km of each other. The “A” and “B” veins have

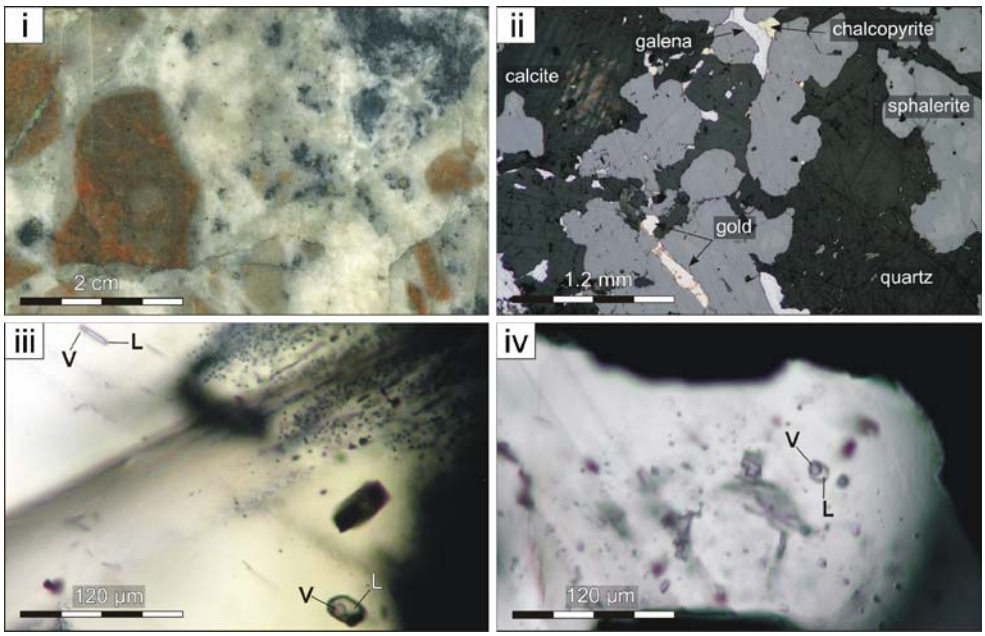

Fig. 6 Stage 2 veins and their fluid inclusions at Shasta. All thin-section photographs were taken in transmitted, plane-polarized light at 25°C, with the exception of photograph (*ii*), which was taken in reflected, plane-polarized light. Abbreviations: *L* liquid, *V* vapor. *i* A stage 2 calcite–quartz–acanthite–pyrite–galena–sphalerite–chalcopyrite vein contains clasts of alkali feldspar-altered lapilli tuff wallrock. *ii* A stage 2 vein contains anhedral grains of cogenetic calcite, quartz, sphalerite, galena, chalcopyrite, and gold. *iii* Translucent, honey-brown sphalerite hosts negative crystal-shaped, aqueous, primary fluid inclusions that are oriented parallel to growth zones in the sphalerite. *iv* Primary, two-phase, liquid-rich, aqueous fluid inclusions are randomly distributed in the center of an undeformed, multiply twinned calcite grain that is rimmed by galena

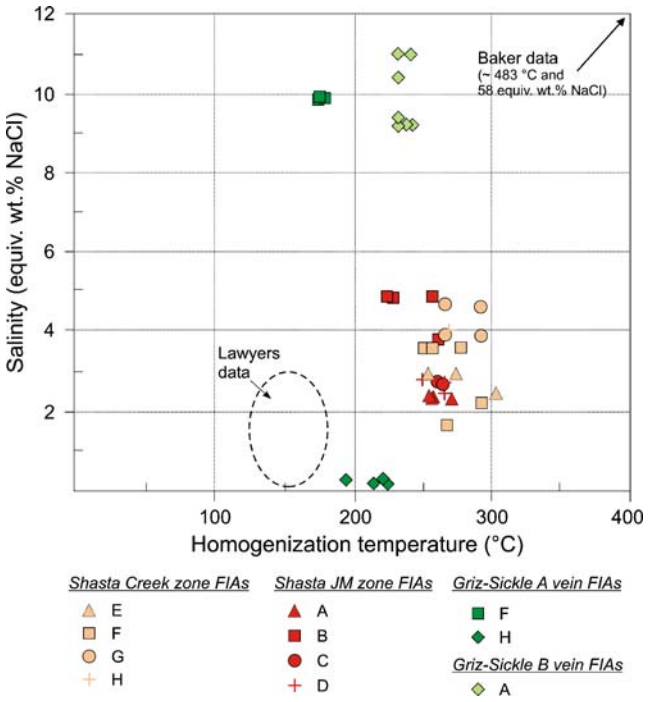

Fig. 7 Salinity and total homogenization temperature data for primary fluid inclusions from low-sulfidation epithermal veins. Two-phase, liquid-rich, aqueous inclusions from Shasta and Griz-Sickle homogenize at temperatures from 175 to 335°C, whereas Lawyers inclusions homogenize at lower temperatures of <180°C (T.J. Reynolds, unpublished report for DuPont of Canada Exploration Ltd., 1983, 9 p.). Inclusions from the Shasta JM and Creek zone orebodies have uniform salinities of 1 to 5 equiv. wt.% NaCl, in contrast to Griz-Sickle fluid inclusions, which can be divided into a <1 and a 9 to 11 equiv. wt.% NaCl group of inclusions. Baker is anomalous in that its primary fluid inclusions include high-temperature, brine-rich, and vapor-rich inclusions

been mined from underground workings and from shallow, 10-m-deep pits that are now inactive. Total production for the A and B veins was 77,500 metric tons of ore yielding 1,168 kg of Au and 23,085 kg of Ag, with a reserve of 50,000 metric tons containing 20.1 g/t Au and 177 g/t Ag (Diakow et al. 1991). Previous studies focused on the vein paragenesis, wallrock alteration, and geochemistry of the A and "West Chappelle" veins (Peter 1983), but include a fluid inclusion study on unmineralized quartz veins from the "C" and West Chappelle veins (T.J. Reynolds, unpublished report for DuPont of Canada Exploration Ltd., 1983, 9 p.). The present study examined three representative diamond drill holes that intersect the A, B, and C veins (Fig. 8), and conducted mapping of structural and hydrothermal alteration relationships in the B vein pit and surrounding outcrop.

The Baker A, B, and C veins cut Takla Group porphyritic basalt, andesite, and rhyodacite. Asitka Group limestone crops out within 200 m of the veins (Figs. 8 and 9 i) and is in fault contact with Takla Group rocks. South of the veins, porphyritic, 196.7±0.3 Ma (Diakow 2006a) granodiorite (Fig. 9 ii) intrudes Asitka Group limestone and Takla Group volcanic rocks. A 20-m-thick block of limestone located along the northern margin of the porphyritic granodiorite about 200 m E of the B vein (Fig. 9 iii) displays strong marbleization and quartz–epidote–garnet skarn alteration (Fig. 9 iv). Several <50-m-thick, ENE-trending syenomonzonite dikes cut Takla Group andesite. Toodoggone Formation volcaniclastic rocks are commonly in fault contact with Takla Group andesite. Both rocks display pervasive epidote–chlorite–calcite±pyrite (i.e., propylitic) alteration.

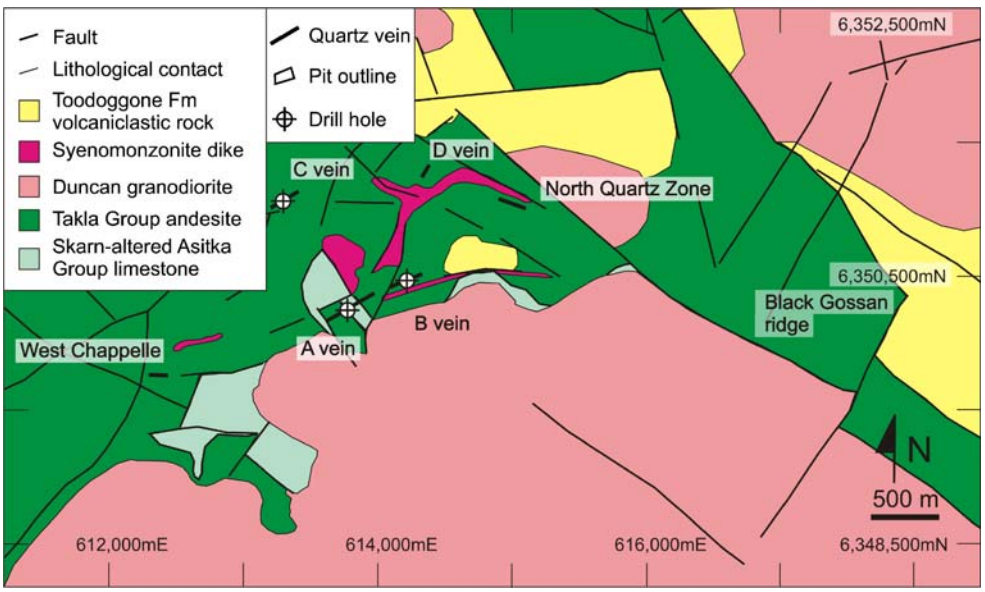

Fig. 8 The simplified geological map of the Baker low-sulfidation epithermal deposit shows the distribution of rock types, structures, and logged diamond drill holes (based on Diakow et al. 1993 and unpublished geological mapping by S. Gower, 1999). The Baker A, B, and C veins are ENE-striking structures that cut Takla Group volcanic rocks. Nearby felsic dikes and porphyritic stocks intrude Takla Group rocks; skarn alteration occurs in Asitka Group limestone units proximal to felsic stocks

The A, B, and C veins are 0.5 to 10 m thick, trend ENE, and extend for strike lengths of up to 440 m and to depths of 150 m. The A vein occurs at the stratigraphic contact between Takla Group plagioclase–quartz–phyric rhyodacite and plagioclase–phyric andesite, whereas the C vein occurs along the contact between rhyodacite and andesite. The B vein occurs along strike and 200 m to the ENE of the A vein (Fig. 8). Chlorite–epidote-altered Takla Group andesite is cut by early <2-cm-thick, banded quartz–magnetite veins, which are in turn cut by the 5-m-thick quartz–sericite–calcite–kaolinite–pyrite–chalcopyrite–acanthite–sphalerite–galena–gold B vein. Within the B vein, milky quartz and pyrite are early-forming mineral phases that are locally cut by cogenetic gray quartz, chalcopyrite, gold, sphalerite, and galena (Fig. 10 i to iii). The B vein and several proximal subparallel veins have steep (80° to 90°) dips and are mostly ENE striking. The veins are offset by steep-dipping, NW-striking faults. The banded quartz–magnetite veins and the B vein are cut by <3-mm-thick, irregularly shaped pyrite–quartz veins. Calcite–zeolite veins cut all vein types. The B vein is surrounded by a 16-m-wide intense quartz–sericite–pyrite proximal alteration zone in andesite. The proximal alteration zones are flanked by kaolinite±pyrite alteration zones. Supergene-related limonite and kaolinite alteration occurs within 25 m of the surface or at deeper depths near the B vein. Supergene fluids caused the oxidation of near-surface rocks and most likely flowed downwards via fractures that cut the subvertical B vein, resulting in the partial weathering of hypogene alteration minerals in wallrock within 15 m of the B vein.

The B vein was selected for fluid inclusion studies because it shows the clearest petrologic relationships and has a comparable vein mineralogy and relative timing to the A and C veins. The B vein records the involvement of two stages of hydrothermal fluid, which precipitated milky quartz followed by gray quartz. Milky quartz is not associated with Au–Ag–Cu mineralization and is commonly fractured, partly recrystallized, and displays undulose extinction. The milky quartz hosts scattered, 1 to 20 μm diameter (a) two-phase, vapor-rich, aqueous inclusions (vapor >90%); (b) two-phase, liquid-rich (liquid >90%) aqueous inclusions; and (c) multiphase, mixed (liquid–vapor–halite) aqueous inclusions. Later-forming gray quartz displays uniform extinction and is cogenetic with chalcopyrite, sphalerite, galena, and gold. Gray quartz hosts 2- to 20-μm-diameter inclusions of chalcopyrite (Fig. 10 iv) in addition to type 1 brine-rich, multiphase (liquid–vapor–halite±sylvite) aqueous inclusions that contain <10% vapor; type 2 multiphase (liquid–vapor±halite) aqueous inclusions that contain 10% to 80% vapor; and type 3

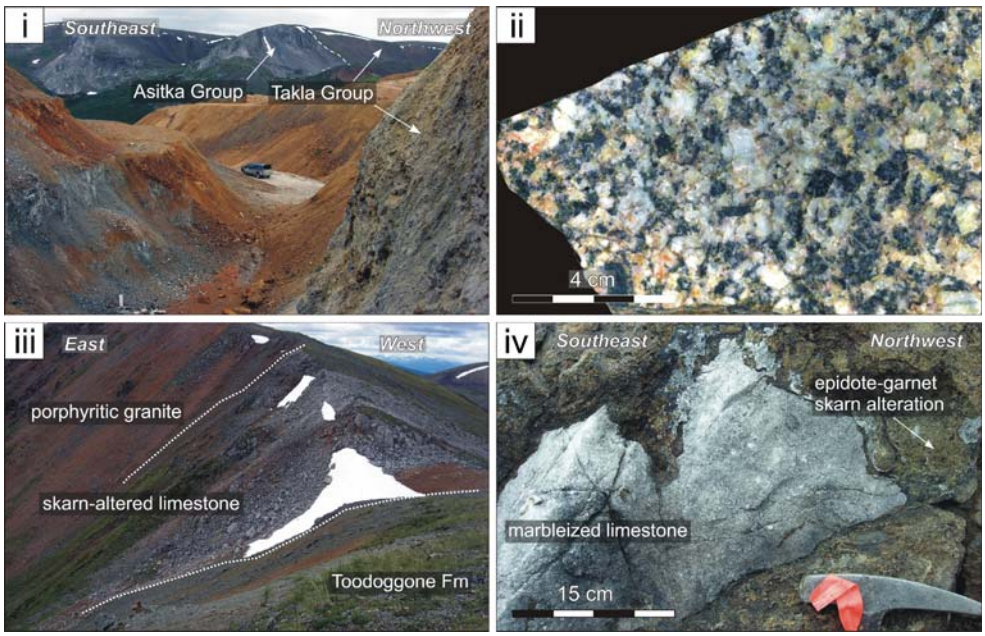

Fig. 9 Photographs of representative rocks at Baker: *i* The Baker B vein is exposed in a 10-m-deep pit that is oriented parallel to the SW-striking vein. Host rocks in the pit are brown, ferruginized Takla Group andesite. In the background hills, slivers of marbleized and locally skarn-altered Asitka Group limestone are overlain by Takla Group volcanic rocks. *ii* Hand specimen of coarse-grained, porphyritic granite that intrudes marbleized limestone. *iii* The 20-m-thick skarn-altered, marbleized Asitka Group limestone has an intrusive lower contact with porphyritic granite. A fault separates the limestone from epidote-altered Toodoggone Formation volcaniclastic rocks. *iv* Slivers of Asitka Group limestone near the contact with the porphyritic granite display recrystallized calcite crystals and local epidote–garnet skarn alteration

vapor-rich, two-phase (liquid–vapor) aqueous inclusions that contain >80% vapor at 25°C. These inclusions occur as scattered clusters in unzoned quartz or locally define pseudosecondary fluid inclusion trails that terminate at grain boundaries (Fig. 10 v and vi). Two-phase (liquid–vapor) aqueous and rare H_2O–CO_2 fluid inclusions define secondary trails that cut gray quartz grain boundaries. Microthermometry data for primary and pseudosecondary fluid inclusion assemblages in gray quartz are presented in Appendix 2.

In summary, measured inclusions are 3 to 20 μm long (mean=12±6 μm, n=19) and 3 to 12 μm wide (mean=7±5 μm, n=19). Eutectic temperatures were not observed in type 3 vapor-rich inclusions; however, final ice melting temperatures range from −2.5 to −0.5 (mean=−1.6±0.9°C, n=4). Final ice melting temperatures correspond to calculated salinities of 0.8 to 4.1 equiv. wt.% NaCl (mean=2.5±1.4 equiv. wt.% NaCl, n=4). The inclusions homogenize to the vapor phase at 355°C (n=2). Type 1 brine-rich inclusions have vapor homogenization temperatures (to the liquid phase) from 291 to 345°C (mean=316±20°C, n=5) and total homogenization temperatures, coinciding with the dissolution of halite daughter crystals, that range from 468 to 507°C (mean=483±14°C, n=5). Salinities calculated using the dissolution temperatures of halite indicate a range from 55.6 to 60.8 equiv. wt.% NaCl (mean=57.7±1.9 equiv. wt.% NaCl, n=5). Dissolution temperatures for sylvite daughter crystals range from 120 to 234°C (mean=176±36°C, n=19).

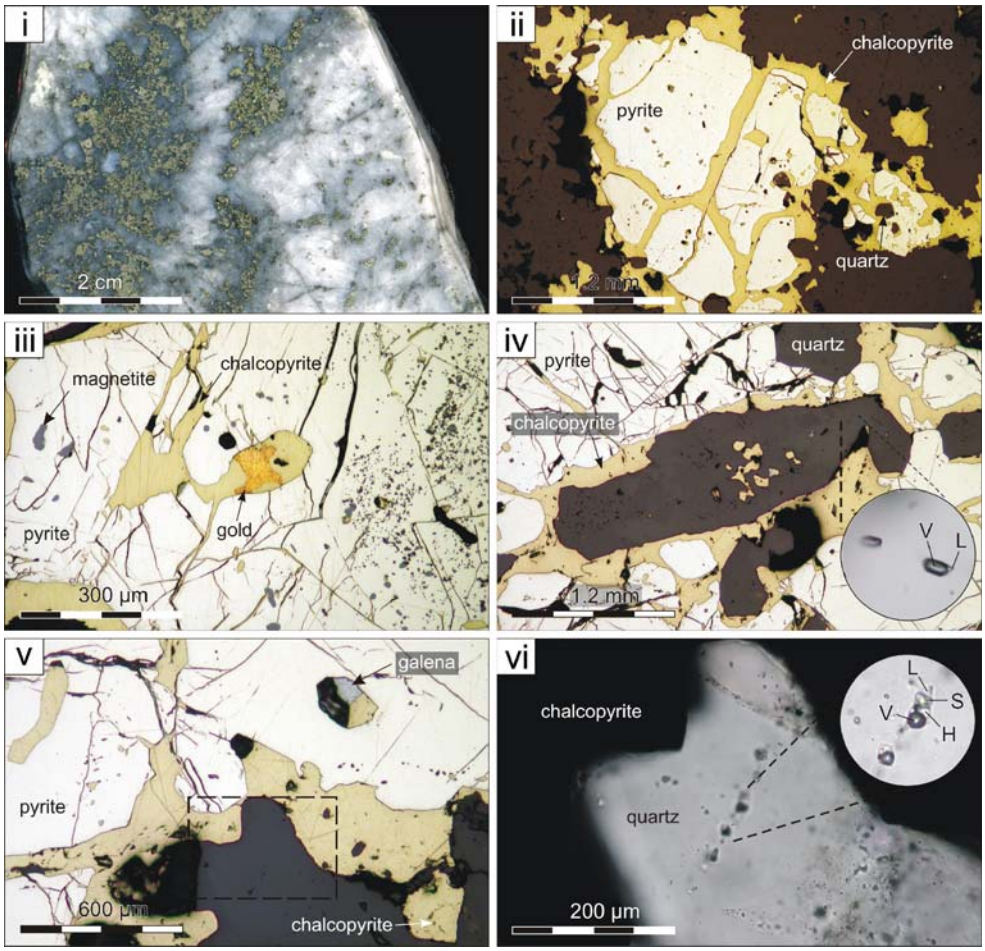

Fig. 10 The Baker B vein and its fluid inclusions. All thin-section photographs were taken in reflected, plane-polarized light at 25°C, with the exception of photograph (*vi*), which was taken in transmitted, plane-polarized light. Abbreviations: *H* halite, *L* liquid, *S* sylvite, *V* vapor. *i* The Baker B vein comprises milky quartz and pyrite that are cut by gray quartz and chalcopyrite. *ii* Pyrite grains are fractured and infilled by chalcopyrite. Cogenetic quartz grains occur as inclusions within chalcopyrite. *iii* Early pyrite with minor magnetite inclusions are cut by chalcopyrite and gold. *iv* Fractures in pyrite are filled by quartz and chalcopyrite. The central elongate quartz grain contains inclusions of chalcopyrite and primary type 3 vapor-rich, and type 1 brine-rich aqueous fluid inclusions. *v* Galena is a minor constituent in the Baker B vein and is cogenetic with chalcopyrite. The *dashed box* shows the position of the magnified photograph in Fig. 10 vi. *vi* Quartz rimmed by chalcopyrite contains a pseudosecondary fluid inclusion trail that includes multiphase-phase, brine-rich, aqueous fluid inclusions

The type 1 brine-rich inclusions homogenize by halite dissolution at temperatures higher than vapor-bubble disappearance temperatures. Consequently, these type 1 brine-rich and type 3 vapor-rich fluid inclusions cannot be immiscible pairs that were trapped in equilibrium (Bodnar 1994; Roedder and Bodnar 1980). Hence, the measured total homogenization temperatures represent minimum trapping temperature estimates. The data suggest that the brine- and vapor-rich inclusions formed during the interaction of at least two fluids of different composition and origin, resulting in the heterogeneous (non-equilibrium) trapping of brine- and vapor-rich fluids. Water leakage from brine-rich inclusions after trapping might also contribute to the tendency for type 1 brine-rich inclusions to homogenize by halite dissolution.

Lawyers

The Lawyers deposit, previously known as Cheni, includes the Amethyst Gold Breccia (reserves of 384,296 metric tons containing 8.64 g/t Au and 250 g/t Ag; Diakow et al. 1991), Cliff Creek (reserves of 1,179,100 metric tons containing 6.05 g/t Au and 243 g/t Ag; Diakow et al. 1991), and Duke's Ridge (reserves of 68,025 metric tons containing

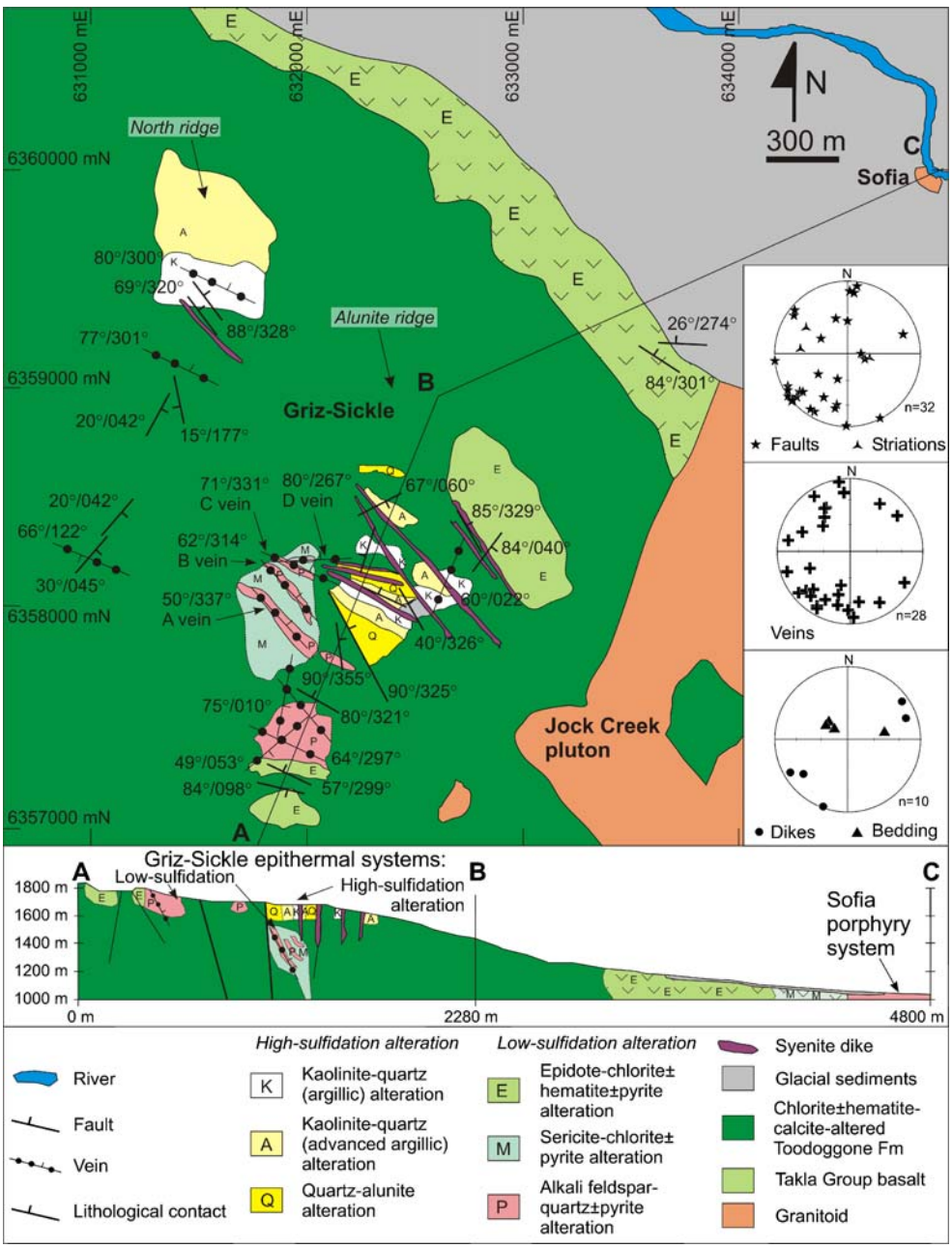

Fig. 11 The simplified geology map shows the distribution of major rock types, hypogene hydrothermal alteration, and major structures for the Griz-Sickle and Sofia prospects. The location of the eastern Jock Creek pluton is based on mapping by Diakow (2006a). The Griz-Sickle area contains examples of high- and low-sulfidation epithermal-style alteration hosted by Toodoggone Formation andesite, all of which are cut by syenite dikes and faults. The SW–NE section (A-B-C) demonstrates the fault truncation of high- and low-sulfidation alteration zones. The lower-hemisphere equal area stereoplots show the orientation of faults, veins, syenite dikes, and sedimentary bedding

7.30 g/t Au and 225 g/t Ag; Diakow et al. 1991) deposits. All are associated with NW-striking, steeply SW-dipping fault zones (Diakow et al. 1991). Previous research at Lawyers includes a reconnaissance fluid inclusion study on a ribboned quartz vein cutting trachyte porphyry and a Au–Ag-bearing quartz vein (T.J. Reynolds, unpublished report for DuPont of Canada Exploration Ltd., 1983, 9 p.). This study examined geological relationships in two 20- and 50-m-long trenches that transect the Amethyst Gold Breccia zone.

The Amethyst Gold Breccia zone is hosted by Toodoggone Formation plagioclase–phyric dacitic tuff. The ore body is 500 m long by 75 m wide and extends to a vertical depth of 150 m (Diakow et al. 1991). The ore body is surrounded by a 25-m-wide alkali feldspar–quartz (i.e., potassic) alteration zone. The age of potassic alteration in the Amethyst Gold Breccia zone is constrained by an Ar–Ar adularia date to be 188.0±1.8 Ma (Clark and Williams-Jones 1991), whereas K–Ar adularia data give a less precise age of 180±6 Ma (Diakow et al. 1991). The central potassic zone is surrounded by a 20-m-thick kaolinite (i.e., argillic) alteration zone, which grades into a 10-m-thick chlorite± epidote±calcite (i.e., propylitic) alteration zone. At least three vein stages are spatially associated with the ore body. Stage 1 veins are NW-striking, <30 cm thick, and contain mainly chalcedonic quartz with minor microcrystalline hematite and rare fine-grained pyrite, electrum, argentite, native gold, native silver, chalcopyrite, sphalerite, and galena (Diakow et al. 1991). Stage 1 veins are cut by <1-m-thick, crustiform-textured stage 2 amethyst–calcite–barite veins and associated hydrothermal breccias that dip moderately to steeply (40° to 90°) to the NE. These veins are cut by subparallel <5-cm-thick stage 3 calcite veins. Brittle faults that strike WSW and SE offset all vein types. Locally, WSW-striking faults display horsetail jog geometries that indicate reverse displacement. A 2-m-thick, moderately dipping, SE-striking, limonite-altered shear zone cuts the western margin of the potassic alteration zone; S and C shear fabric relationships within the shear zone indicate reverse movement. A stage 2 ribboned quartz vein contains low-temperature (<180°C), low-salinity (<3 equiv. wt.% NaCl) primary fluid inclusions (T.J. Reynolds, unpublished report for DuPont of Canada Exploration Ltd., 1983, 9 p.).

Griz-Sickle

The Griz-Sickle low-sulfidation epithermal Au–Pb–Zn±Ag system is located 5 km SW of the Sofia porphyry Au–Cu± Mo prospect (Fig. 11) and about 300 m W and 100 m lower in elevation than high-sulfidation epithermal-style alteration and mineralization (Fig. 12 i). It consequently presents a

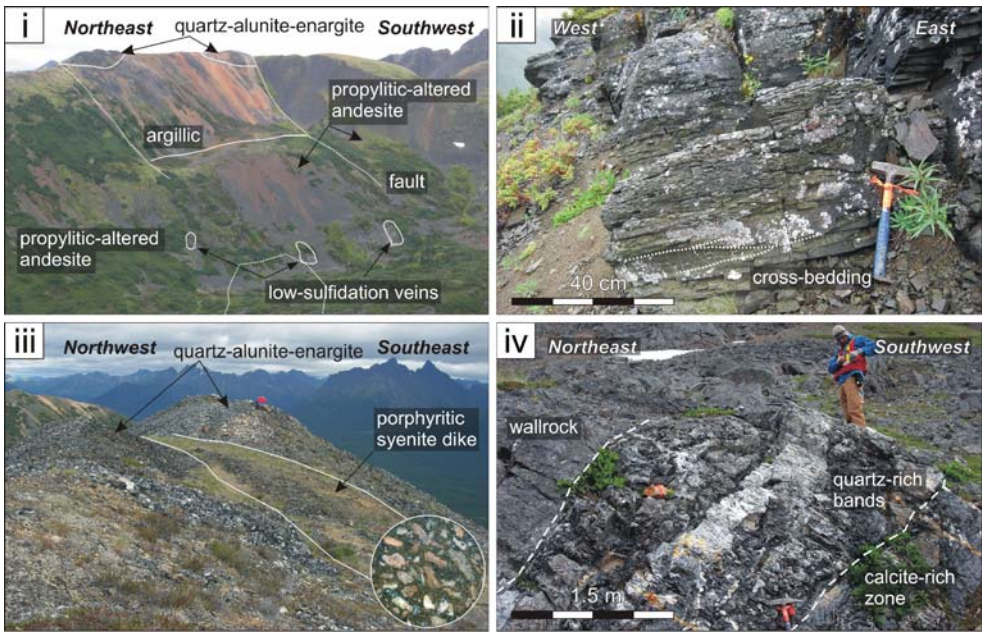

Fig. 12 Photographs of representative rocks at Griz-Sickle: *i* High-sulfidation epithermal alteration in Toodoggone Formation andesite crops out along the top of Alunite ridge and overlies low-sulfidation epithermal veins and alteration. The north and south margins of the high-sulfidation-style alteration zones are defined by steep-dipping, NW-striking faults. Alunite ridge is 200 to 250 m high. *ii* Host rocks in the Griz-Sickle area include a medium- to coarse-grained, well-sorted, chloritic sandstone that locally displays shallowly WSW-dipping planar and cross beds. *iii* All rock types and the high-sulfidation quartz–alunite alteration zones in Alunite ridge are cut by fresh, NW-striking, alkali feldspar–phyric syenite dikes. The *inset photograph* shows a 2-cm-diameter hand specimen of the syenite dike. *iv* The Griz-Sickle A vein is 1 to 5 m thick and contains alternating ribbons of quartz- and calcite-rich zones. The wallrock to the A vein is a plagioclase–phyric andesite that is altered to quartz and alkali feldspar

good area for testing genetic relationships between porphyry and different styles of epithermal systems in the district. The present study included 1:1,000-scale mapping of major rock types, structures, and alteration styles in the Griz-Sickle to Sofia area. Least-altered rocks in the Griz-Sickle area include mainly Toodoggone Formation andesite lavas, sills, and volcaniclastic rocks, with minor epiclastic siltstone, sandstone, and conglomerate units that crop out in the SW of the map area. Bedding in the sandstone and conglomerate dips about 30° to the SE (Figs. 11 and 12 ii). Least-altered Toodoggone Formation andesite is moderately altered to chlorite and hematite. All rock types are intruded by 1- to 10-m-thick, steep-dipping, NW-trending porphyritic syenite dikes (Fig. 12 iii). The ca. 196.7±0.3 Ma (Diakow 2006a) Jock Creek pluton crops out about 1 km east of epithermal-style mineralization in the NE-trending "Alunite ridge" (Fig. 11).

Low-sulfidation epithermal alteration and mineralization zones occur in the south-central area of the prospect and are associated with NW- and NE-striking quartz–calcite–alkali feldspar±galena±chalcopyrite±sphalerite±pyrite veins (Fig. 11). The Griz-Sickle "A", "B", "C", "D", and "E" veins exposed at the base of Alunite ridge (Figs. 11 and 12 i) are 1 to 5 m thick, 5 to 50 m long, and display well-developed banding of quartz- and calcite-rich zones (Fig. 12 iv). Quartz-rich zones display euhedral quartz crystals and lattice textures, whereas calcite-rich bands contain coarse-grained, platy calcite crystals, abundant vugs, and inclusions of wallrock fragments proximal to vein margins. Galena, sphalerite, pyrite, and chalcopyrite are mainly concentrated in calcite-rich bands within 0.5 m of vein margins. These areas have metal grades of up to 0.4 ppm Au and 221 ppm Ag (over 2.6 m). A dacite dike that cuts Toodoggone Formation andesite and the A vein has a U–Pb zircon age of 188.7±0.8 Ma (Diakow 2006a).

Proximal porphyritic andesite wall rock to the A to E veins is pink and quartz–alkali feldspar±pyrite-altered. The 10- to 20-m-thick potassic alteration zones contain well-developed, 1- to 3-cm-thick stockwork quartz–calcite±pyrite veins that decrease in frequency with distance from the main veins. Potassic alteration zones grade into 20- to 30-m-thick quartz–sericite±pyrite (i.e., phyllic) alteration zones, which in turn grade into distal chlorite–epidote (i.e., propylitic) alteration zones. Epidote–chlorite±pyrite alter-

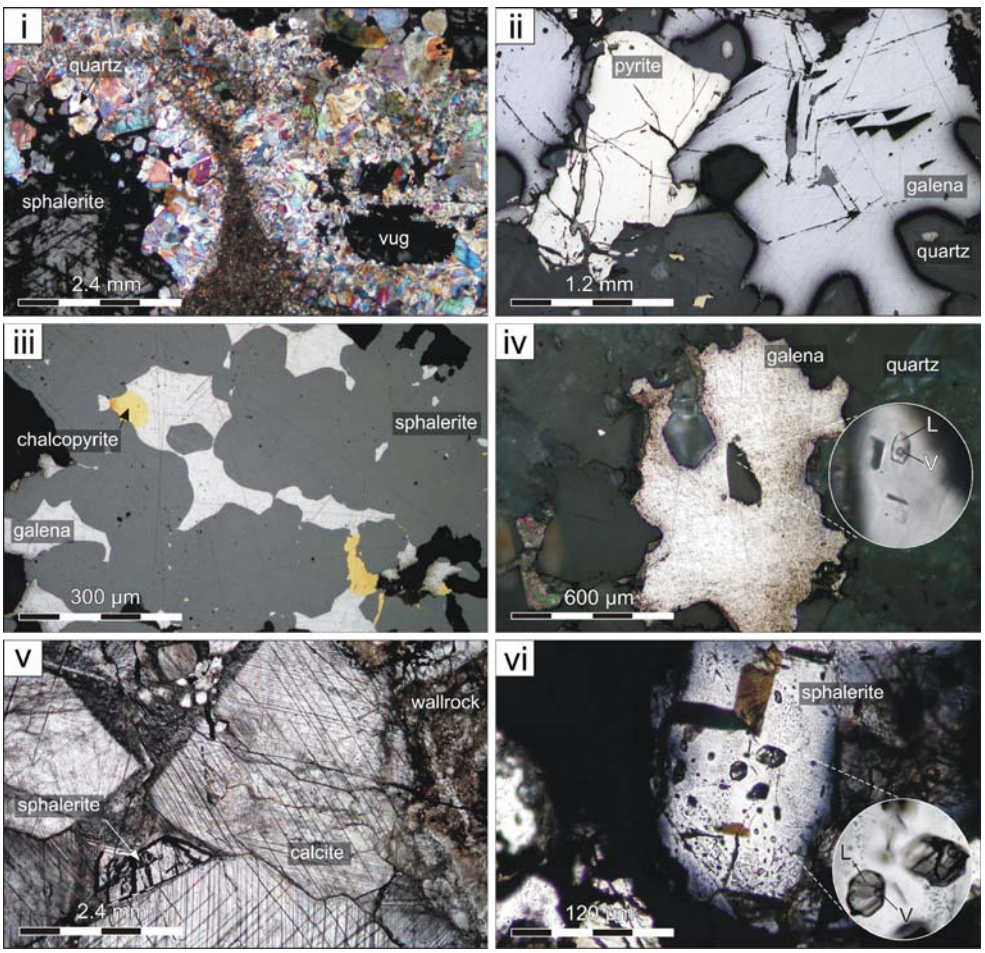

Fig. 13 Griz-Sickle A and B veins and their fluid inclusions. All thin-section photographs were taken in reflected, plane-polarized light at 25°C, with the exception of photographs (*v*) and (*vi*), which were taken in transmitted, plane-polarized light. Photograph (*i*) was taken in cross-polarized light. Abbreviations: *L* liquid, *V* vapor. *i* Sphalerite, euhedral quartz, and calcite occur in the center of vugs in the A vein. The margins of vugs are defined by fine-grained quartz. *ii* Cogenetic pyrite and galena are intergrown with quartz in the B vein. *iii* Sphalerite is intergrown with cogenetic galena, chalcopyrite, and quartz in the B vein. *iv* An anhedral galena grain hosts inclusions of quartz in the A vein. The quartz contains several 15-µm-long, primary, two-phase liquid-rich aqueous fluid inclusions. *v* A vug in the B vein is filled by coarse-grained, euhedral calcite, quartz, and translucent sphalerite. *vi* Translucent sphalerite from the B vein hosts several <30 µm diameter, liquid-rich, primary fluid inclusions

ation in Toodoggone Formation andesite is well developed to the NE of the Griz-Sickle epithermal systems and is most pronounced in Takla Group basalt proximal to the Sofia porphyry Au–Cu±Mo prospect (Fig. 11). Glacial sediments cover most of the area between Griz-Sickle and Sofia, which prevents an accurate assessment of the type and extent of alteration zonation around the Sofia porphyry system.

Low-sulfidation-style quartz veins also crop out on the crest of Alunite ridge, about 500 m to the S and 200 m above the A to E veins (Fig. 11). At this location, the veins strike NE and NW, are narrower (1 to 10 cm thick), and contain minor calcite and trace pyrite. Adularia from a potassic alteration halo to the veins has an Ar–Ar age of 190.0±1.3 Ma (Diakow et al. 2006). These veins are separated from the A to E veins by a steep-dipping, NW-striking fault. Brittle faults mostly dip steeply (85°) to the NE, strike NW, and are oriented subparallel to quartz–calcite veins and syenite dikes (Fig. 11). A second less-common fault set dips steeply to the SE (i.e., 80°/095°).

Eight doubly polished thin sections of the Griz-Sickle A, B, C, and D veins were studied and microthermometry was performed on one sample each of the A and B veins. Pyrite, galena, sphalerite, chalcopyrite, quartz, and calcite in the veins are cogenetic (Fig. 13 i, ii, and iii). Quartz used for microthermometry displays uniform extinction and commonly rims, or is surrounded by, galena (Fig. 13 iv) or sphalerite. Translucent sphalerite often occurs in the center of calcite-filled vugs (Fig. 13 v). Two-phase (liquid-rich) aqueous primary fluid inclusions that are equant to elongate and negative crystal-shaped are present in the center of unzoned quartz (Fig. 13 iv) or in zoned sphalerite (Fig. 13 vi). Pseudosecondary fluid inclusions in sphalerite have a similar morphology and composition to primary inclusions but occur as trails that terminate at sphalerite grain boundaries. Microthermometry data for fluid inclusion assemblages measured from the A and B veins are presented in Appendix 2 and Fig. 7.

Measured primary inclusions in the A and B veins are 2 to 30 μm long (mean=12±8 μm, n=38) and 2 to 25 μm wide (mean=8±6 μm, n=38). Only one eutectic temperature was measured for primary fluid inclusions in the A vein; the T_e of −23.3 is below the eutectic temperature for the H_2O–NaCl system (i.e., −20.8°C) and indicates the presence of dissolved salts other than NaCl (Shepherd et al. 1985). No CO_2 was detected in any fluid inclusion. Final ice melting temperatures for inclusions in the A vein range from −6.5 to −0.1 (mean=−2.3±3.3°C, n=6), whereas T_m for inclusions in the B vein have a more restricted range from −7.4 to −6.0 (mean=−6.7±0.5°C, n=11). Final ice melting temperatures for inclusions in the A vein correspond to calculated salinities of 0.2 to 9.8 equiv. wt.% NaCl (n=6), with data clustering in two distinct populations. In comparison, calculated salinities for inclusions in the B vein have a tighter range from 9.2 to 11.0 equiv. wt.% NaCl (mean=10.1±0.7 equiv. wt.% NaCl, n=11). Primary inclusions in the A and B veins homogenize to the liquid phase; temperatures range from 175 to 224°C (mean=195±18°C, n=13) for the A vein and 233 to 242°C (mean=236±4°C, n=8) for the B vein.

Platy calcite crystals and quartz lattice textures located along the margins and in the center of the banded Griz-Sickle A and B veins suggest that the hydrothermal fluids underwent repeated episodes of boiling during vein formation (e.g., Simmons and Browne 2000). Although no coeval vapor-rich and liquid-rich aqueous primary fluid inclusions were observed in quartz or sphalerite grains in this study, the bimodal salinity ranges demonstrated by primary fluid inclusions in the A vein suggest fluid boiling and/or mixing occurred (e.g., Hayba 1997; Hedenquist and Henley 1985). Assuming that the hydrothermal fluids for the A and B veins were boiling at the time of metal deposition, total homogenization temperatures represent true trapping temperatures. Corresponding trapping pressures from the A vein are 20 to 30 bar, which equate to lithostatic depths of 65 to 100 m, assuming a lithostatic pressure gradient of 3.3 km/1 kb (Hagemann and Brown 1996), or hydrostatic depths of 200 to 300 m, assuming a hydrostatic pressure gradient of 100 bar/km. Trapping pressures for the B vein are lower at about 12 bar, which corresponds to a lithostatic depth of about 40 m or a hydrostatic depth of about 120 m, using the assumptions above.

High-sulfidation systems

Griz-Sickle

High-sulfidation epithermal mineralization occurs in Toodoggone Formation porphyritic andesite along the NE-trending crest of Alunite ridge and at the northern extremity of the "North ridge" (Figs. 11 and 12 i). Alteration exposed along Alunite ridge is concentrically zoned in places and includes a central 80-m-wide quartz–alunite±enargite±dickite±illite±pyrophyllite alteration zone bordered by a 60-m-wide kaolinite–quartz–illite (i.e., advanced-argillic) alteration zone, which grades into a 50-m-wide kaolinite–quartz (i.e., argillic) zone, and then a chlorite–epidote-altered andesite. The central quartz–alunite±enargite±dickite±illite±pyrophyllite alteration zone defines a 10-m-thick competent horizon that contains Au and Cu concentrations of up to 0.98 ppm and 536 ppm, respectively; primary igneous textures are completely replaced by alteration minerals. Advanced-argillic alteration zones are less competent and display remnant

igneous porphyritic textures. Argillic alteration zones have a remnant porphyritic texture and contain igneous plagioclase, amphibole, and biotite.

Northern and southern limits of high-sulfidation epithermal alteration on Alunite ridge coincide with NW-striking faults, which juxtapose quartz–alunite±enargite±dickite±illite±pyrophyllite alteration zones with chlorite–hematite-altered andesite (Fig. 12 i). High-sulfidation epithermal alteration extends to a vertical depth of about 100 m below the present surface on Alunite ridge, whereas the A to E low-sulfidation veins crop out a further 100 m below the limits of high-sulfidation alteration (Fig. 12 i). Alunite from quartz–alunite

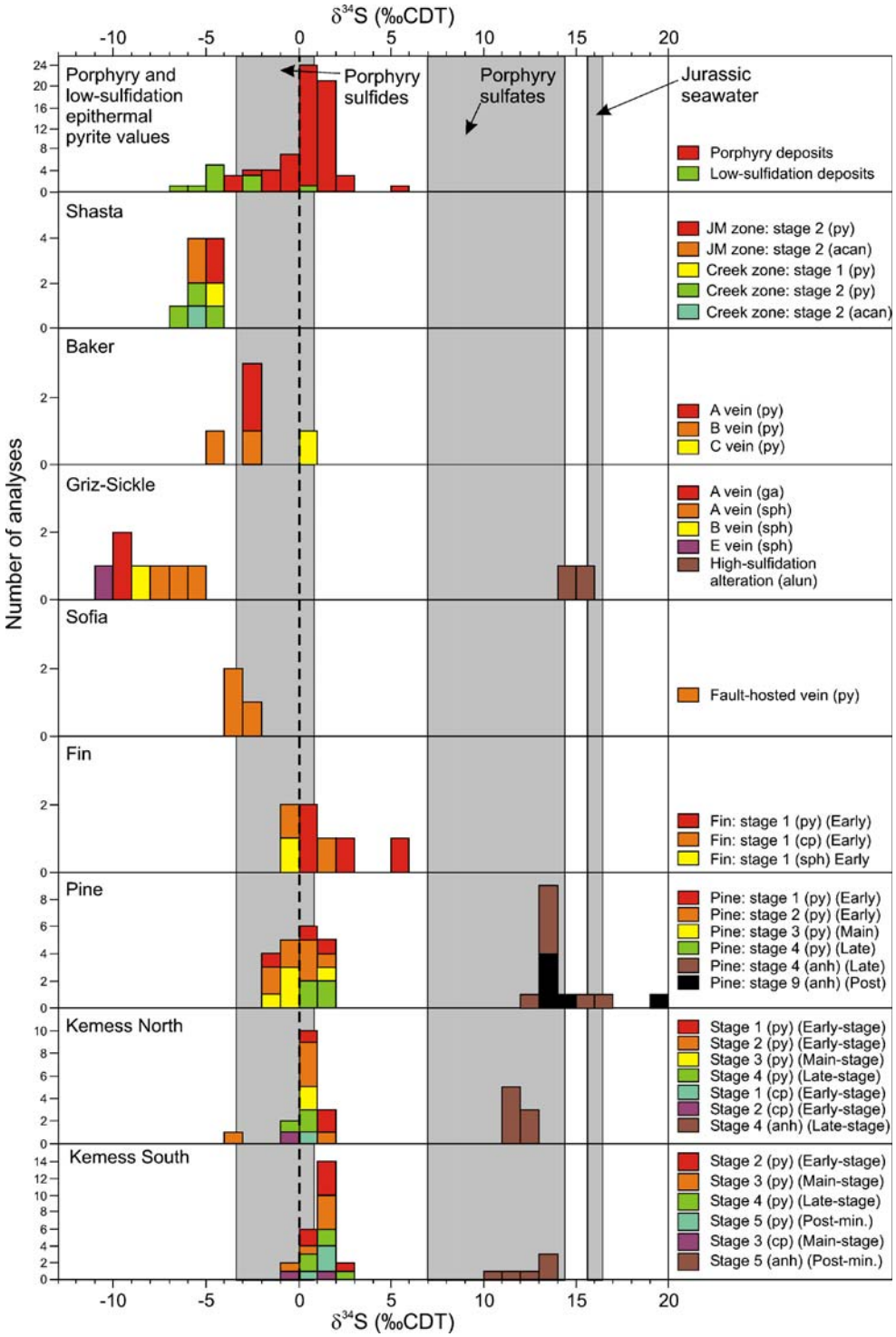

Fig. 14 Frequency histogram plots of $\delta^{34}S$ values for sulfide and sulfate minerals from representative porphyry Cu–Au±Mo and epithermal Au±Ag systems in the Toodoggone district. Kemess South data are from Duuring et al. (2008), whereas Kemess North and Pine/Fin data are from McKinley (2006) and Dickinson (2006), respectively. Sulfur isotope values for all porphyry Cu–Au±Mo examples overlap the $\delta^{34}S$ value range for porphyry-related sulfide and sulfate minerals, as defined by Rollinson (1993). The $\delta^{34}S$ range for Jurassic seawater sulfur (Claypool et al. 1980) is also shown for reference. Abbreviations: *acan* acanthite, *alun* alunite, *anh* anhydrite, *cp* chalcopyrite, *ga* galena, *py* pyrite, *sph* sphalerite

±enargite±dickite±illite±pyrophyllite alteration zones in Alunite ridge give an Ar–Ar age of 196.9±2.2 Ma (Diakow et al. 2006), indicating that high-sulfidation alteration is coeval with the emplacement of the nearby Jock Creek pluton (i.e., 196.7±0.3 Ma) but is at least 3.4 million years older than low-sulfidation alteration (i.e., 190.0±1.3 Ma). Both high- and low-sulfidation epithermal alteration zones are locally cut by unaltered porphyritic syenite dikes.

Silver Pond

The Silver Pond high-sulfidation epithermal system is located about 3 km west of the low-sulfidation system Amethyst Gold Breccia zone and is characterized by a central quartz–dickite± pyrite±barite alteration zone (Diakow et al. 1991, 1993). Microcrystalline quartz contains irregular cavities and narrow open fractures lined by druse quartz. These central zones are surrounded by dickite–quartz±natroalunite (i.e., argillic) zones, which grade outwards into chlorite–carbonate–epidote±montmorillonite (i.e., propylitic)- altered Toodoggone Formation rocks (Diakow et al. 1993).

Al

The Al deposit is located 20 km N of Silver Pond and hosts the Bonanza, BV, and Thesis zones. The ore zones are elongate (<2.5 km long by <500 m wide) and are associated with N- to NW-trending faults that cut shallowly S- to SW-dipping Toodoggone Formation dacite (Clark and Williams-Jones 1986; Diakow et al. 1993). All zones have a central mineralized area that is comprised chiefly of quartz and barite breccias and veins, and includes minor gold, pyrite, electrum, tetrahedrite, argentite, chalcopyrite, galena, and sphalerite (Diakow et al. 1991). The central silica-rich zones are commonly enveloped by quartz–natroalunite–dickite (i.e., advance-argillic) alteration zones, which grade outwards into quartz–illite–hematite (i.e., argillic) zones (Clark and Williams-Jones 1986, 1989; Diakow et al. 1993). The Bonanza zone differs in that sericite is abundant and advanced-argillic alteration is absent. Sericite from the Bonanza zone gives an interpreted Ar/Ar date of ca. 196 Ma for high-sulfidation-style mineralization (Clark and Williams-Jones 1991). Primary fluid inclusions in barite from quartz–barite–gold veins from the Verrenass zone of the Al deposit have total homogenization temperatures of 180 to 200°C and salinities of about 3 equiv. wt.% NaCl (Clark and Williams-Jones 1986).

Sulfur isotope data

Sulfur isotope data are elsewhere reported for the Kemess South (Duuring et al. 2008), Kemess North (McKinley 2006), and the Pine and Fin (Dickinson 2006) porphyry Cu–Au±Mo systems. This study compares these with new $\delta^{34}S_{sulfide}$ data for metalliferous veins from the Sofia, Griz-Sickle, Baker, and Shasta systems (Appendix 3, Fig. 14). No S isotope data were obtained from the Lawyers Amethyst Gold Breccia zone or from Silver Pond due to the rarity and fine grain size of sulfide minerals; for similar reasons, only alunite was analyzed from high-sulfidation epithermal alteration zones at Griz-Sickle.

The $\delta^{34}S_{sulfide}$ values for early-, main-, late-, and post-mineralization-stage veins from the Kemess South (−0.3‰ to 2.9‰, n=26), Kemess North (−3.2‰ to 1.4‰, n=16), Pine (−1.9‰ to 1.7‰, n=20), and Fin (−0.9‰ to 5.6‰, n=7) porphyry systems overlap the −3.5‰ to 1.0‰ $\delta^{34}S_{sulfide}$ range exhibited by most porphyry deposits (Rollinson 1993) and suggests that S, and perhaps metals, were mainly derived from magmatic fluids, which have $\delta^{34}S_{H2S}$ values of about 0‰ (Ohmoto 1986; Taylor 1987). Anhydrite in late- to post-mineralization-stage veins from the studied porphyry Cu–Au–Mo deposits have $\delta^{34}S_{anhydrite}$ values that range from 11.0‰ to 19.7‰ (n=28), which overlaps the 9.0‰ to 14.5‰ range displayed by most porphyry deposits (Rollinson 1993). With the exception of Pine and Fin, $\delta^{34}S_{anhydrite}$ values for porphyry systems are lower than the average value for Jurassic seawater ($\delta^{34}S$ ~16‰; Claypool et al. 1980), which suggests only minor mixing between magmatic-derived ore fluids and Jurassic seawater. Cogenetic pyrite from late- to post-mineralization-stage anhydrite–pyrite veins have $\delta^{34}S_{pyrite}$ values that range from −1.9‰ to 1.9‰. Calculated initial unfractionated S isotope fluid compositions ($\delta^{34}S_{\Sigma S}$) for these veins range from 2.2‰ to 9.1‰. At Sofia, early-forming quartz–magnetite±alkali feldspar veins associated with potassic alteration in the granodiorite do not contain significant concentrations of sulfide minerals. Later-forming, fault-hosted Cu–Au veins have $\delta^{34}S_{pyrite}$ values that range from −3.6‰ to −2.2‰ (n=3). These values are more negative than most $\delta^{34}S_{pyrite}$ data from Kemess South, Kemess North, Pine, and Fin (Fig. 14).

Gold±Ag veins from low-sulfidation epithermal systems in the district have $\delta^{34}S_{sulfide}$ values that are more negative than $\delta^{34}S_{sulfide}$ values for metalliferous veins from porphyry Au–Cu±Mo deposits (Fig. 14). For example, Griz-Sickle A, B, and E veins have $\delta^{34}S_{sulfide}$ values for galena and sphalerite that range from −10.9‰ to −5.9‰ (n=7); Baker A, B, and C veins have $\delta^{34}S_{pyrite}$ values that range from −4.8‰ to 0.1‰ (n=5); whereas Shasta stage 1 and 2 veins have $\delta^{34}S_{sulfide}$ values for pyrite and acanthite that range from −6.4‰ to −4.5‰ (n=9). The more negative $\delta^{34}S_{sulfide}$ values for low-sulfidation epithermal veins might be a consequence of the ore fluid interacting with an external, isotopically negative S source, such as biogenic sulfide minerals. However, considering that the examined epithermal deposits are widely spaced in the district and no

sedimentary sulfide minerals were observed in any exposed country rocks to the epithermal deposits, it is more likely that the negative $\delta^{34}S_{sulfide}$ values are the result of hydrothermal fluid boiling. Fluid boiling, such as that which occurred at Shasta and Griz-Sickle, probably corresponded with a loss in H_2 and the oxidation of the ore fluids (e.g., Drummond and Ohmoto 1985). The removal of H_2S via oxidation to SO_4 caused residual aqueous H_2S to be depleted in ^{34}S and resulted in negative shifts in $\delta^{34}S$ for sulfide minerals that precipitated from the fluids (e.g., McKibben and Eldridge 1990; Rye 1993; Rye et al. 1992).

Baker veins display the most positive $\delta^{34}S_{sulfide}$ values compared with other low-sulfidation epithermal veins in the district. The values overlap the typical range for porphyry deposits (i.e., −4‰ to 1‰; Rollinson 1993) and suggest that the Baker ore fluid had a magmatic source. In contrast, boiling of the ore fluids during metal deposition at Shasta and Griz-Sickle resulted in negative shifts in $\delta^{34}S_{sulfide}$ values and difficulties in interpreting the source of the ore fluids.

Carbon and oxygen isotope data

Carbon and O isotope data exist for the Kemess South (Duuring et al. 2008), Kemess North (McKinley 2006), and the Pine and Fin (Dickinson 2006) porphyry Cu–Au±Mo systems. Thiersch et al. (1997) report $\delta^{18}O_{fluid}$ values for hydrothermal quartz and calcite from Shasta Ag–Au-bearing epithermal veins, whereas Diakow et al. (1991) give $\delta^{18}O$ and $\delta^{13}C$ data for calcite from Lawyers and Silver Pond as well as whole-rock isotope values for regional zeolite-facies metamorphic minerals in volcanic country rock from throughout the district. This study presents C and O isotope data for calcite from least-altered Asitka Group limestone at Baker as well as hydrothermal calcite from main- and post-mineralization-stage veins from the Griz-Sickle, Baker, Shasta, and Lawyers low-sulfidation epithermal systems (Appendix 4).

Calcite from least-altered Asitka Group limestone at Kemess South, Kemess North, and Baker have $\delta^{13}C_{calcite}$ values that range from 0.4‰ to 5.2‰ (n=7), which is comparable with recognized $\delta^{13}C_{calcite}$ values for marble and unaltered limestone (i.e., about −3‰ to 4‰; Sharp 2006). Corresponding Asitka Group limestone $\delta^{18}O_{calcite}$ values range from 3.6‰ to 21.6‰ but are mostly lower than the reported range of $\delta^{18}O_{calcite}$ values for marble and unaltered limestone (i.e., about 15‰ to 30‰; Sharp 2006). The low $\delta^{18}O_{calcite}$ values are most likely the result of the limestone interacting with meteoric, metamorphic, and/or magmatic fluids.

Methane was not observed in trapped primary fluid inclusions in any veins and its presence is assumed to be negligible, with CO_2 being the dominant carbon species in the hydrothermal fluids. $\delta^{13}C_{CO2}$ values for the veins are calculated using fluid trapping temperatures obtained from microthermometry for each mineralizing system and using the calcite–CO_2 fractionation equation of Ohmoto and Rye (1979). The $\delta^{18}O_{H2O}$ values for veins are estimated using the calcite–H_2O fractionation equation of O'Neil et al. (1969).

Kemess South is the only porphyry deposit in the district that has C and O isotope data available for early- and main-stage Cu–Au±Mo veins. Assuming a trapping temperature of 380°C for these veins, calculated $\delta^{13}C_{CO2}$ values range from −1.2‰ to 3.2‰, whereas calculated $\delta^{18}O_{H2O}$ values range from 6.1‰ to 9.0‰ (Duuring et al. 2008). The $\delta^{13}C_{CO2}$ and $\delta^{18}O_{H2O}$ values overlap the respective isotope values for Kemess South Asitka Group limestone that was in equilibrium with hydrothermal fluids at 380°C (Fig. 15). Thus, magmatic–hydrothermal fluids released from the Maple Leaf granodiorite at Kemess South probably interacted with proximal limestone country rock, which resulted in a positive shift in the $\delta^{13}C_{CO2}$ value for the ore fluids. Assimilation of limestone during granodiorite emplacement might also explain the positive shift in $\delta^{13}C_{CO2}$ values for the magmatic-derived ore fluid.

Post-mineralization-stage calcite-rich veins at Kemess South, Kemess North, Pine, and Fin formed at about 200°C (Dickinson 2006; Duuring et al. 2008; McKinley 2006). At Kemess South, post-mineralization-stage veins have calculated $\delta^{13}C_{CO2}$ and $\delta^{18}O_{H2O}$ values that are comparable with limestone in equilibrium with a hydrothermal fluid at 200°C (Fig. 15). Thus, post-mineralization-stage fluids at Kemess South most likely interacted with limestone prior to vein formation. In contrast, post-mineralization-stage veins at Kemess North and Pine have $\delta^{13}C_{CO2}$ values that are significantly lower. These post-mineralization-stage veins in these deposits did not experience the same degree of fluid interaction with limestone country rock as at Kemess South.

Low-sulfidation epithermal Au±Ag veins at Griz-Sickle and Shasta have $\delta^{13}C_{CO2}$ and $\delta^{18}O_{H2O}$ values with positive linear trends. Positive values for Shasta veins are most comparable with limestone values, whereas the negative values for the Shasta and Griz-Sickle veins are similar to isotope values for meteoric fluids. The isotope trends indicate that meteoric fluids at Griz-Sickle and Shasta interacted with limestone and siliceous country rocks and reached various levels of equilibration. The strongly negative $\delta^{13}C_{CO2}$ values at Lawyers are probably the result of interaction between meteoric/metamorphic fluids and organic C in sedimentary country rock. Well-bedded, >200-m-thick epiclastic rocks are mapped 1.5 km south of the Amethyst Gold Breccia zone (Diakow et al. 1993) and may have been a source of organic C. In

contrast to the other low-sulfidation epithermal deposits, Baker A and B veins have $\delta^{13}C_{CO2}$ and $\delta^{18}O_{H2O}$ values that are most comparable with isotope ratios for Kemess South early- and main-stage veins (Fig. 15). Furthermore, the Baker A vein has $\delta^{13}C_{CO2}$ and $\delta^{18}O_{H2O}$ values that are similar to values for limestone that is in equilibrium with hydrothermal fluids at 483°C. Hence, the Baker ore fluids were most likely derived from a magma but re-equilibrated with limestone country rock, resulting in a positive shift in $\delta^{13}C_{CO2}$ values without significantly changing the $\delta^{18}O_{H2O}$ values of the ore fluid.

Radiogenic lead isotope data

Lead isotope studies exist for Kemess North (McKinley 2006) as well as Pine and Fin (Dickinson 2006). In this study, Pb isotope values were determined for calcite, plagioclase, and alkali feldspar separates from least-altered Asitka Group, Takla Group, Toodoggone Formation, and plutonic rocks from throughout the district. Sulfide minerals were analyzed from porphyry Cu–Au±Mo and epithermal Au±Ag systems (Appendix 5) with the aim of constraining the source of metals in each system.

Country rocks to mineral deposits

Asitka Group limestone data plot in two groups: radiogenic samples from Kemess South, and less radiogenic samples from Baker (Fig. 16 i). The highly radiogenic Kemess South signature might be that of Permian seawater or due to inclusions of fine-grained clastic material in the limestone. Correlation of Asitka Group limestone with other rocks or vein samples is hindered because the Pb isotope values for the limestone are not age corrected. In general terms, Pb isotope values for Takla Group basalt are more radiogenic

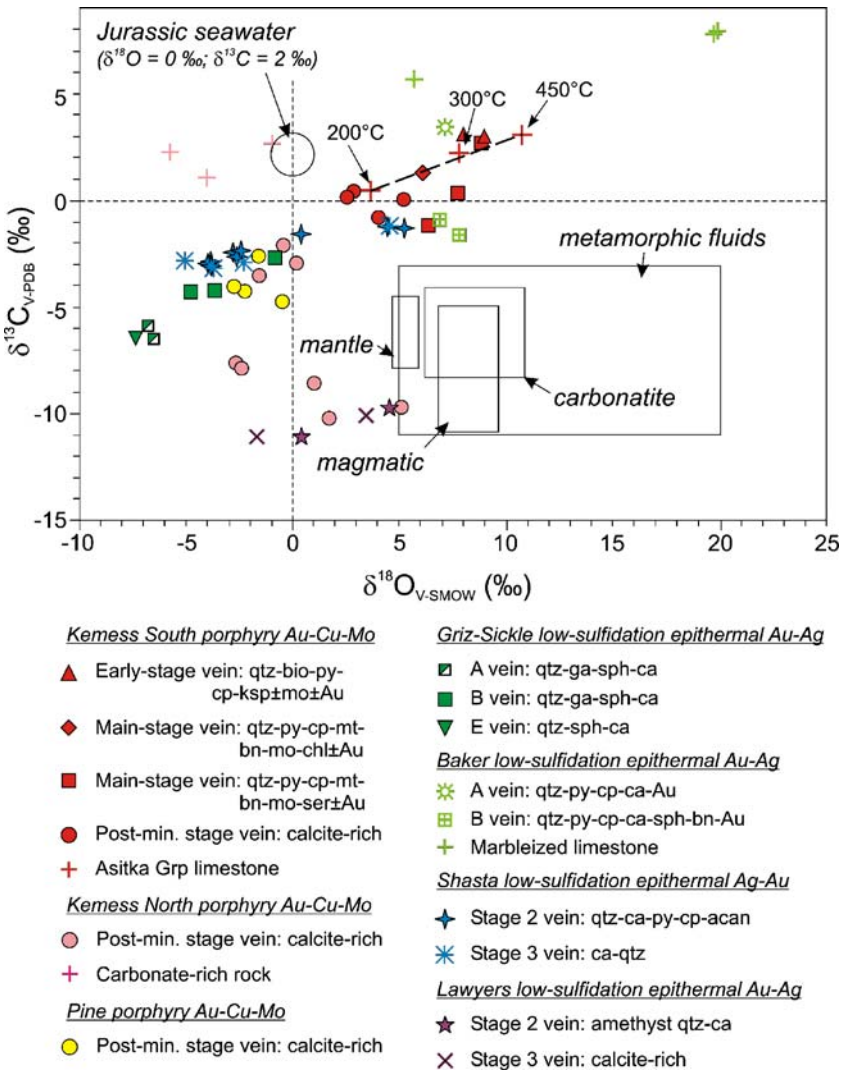

Fig. 15 Carbon and oxygen isotope fluid values are presented for Asitka Group limestone and veins from porphyry Cu–Au–Mo deposits and low-sulfidation epithermal Au±Ag deposits in the Toodoggone district. Calculated $\delta^{13}C_{CO2}$ and $\delta^{18}O_{H2O}$ values are plotted for a Kemess South Asitka Group limestone sample that is in equilibrium with hydrothermal fluids at 200, 300, and 450°C. The Baker and Kemess North limestone isotope values are calculated for limestone samples that are in equilibrium with hydrothermal fluids at 483°C (for Baker) or 200°C (for Kemess North). Isotope data from the Kemess North and Pine deposits are for post-mineralization-stage veins (Dickinson 2006; McKinley 2006). *Line boxes* represent data fields reported by Sharp (2006). The Jurassic seawater values are from Veizer et al. (1999). Abbreviations: *acan* acanthite, *bio* biotite, *bn* bornite, *ca* calcite, *chl* chlorite, *cp* chalcopyrite, *ga* galena, *ksp* alkali feldspar, *mo* molybdenite, *mt* magnetite, *py* pyrite, *qtz* quartz, *ser* sericite, *sph* sphalerite

than the average Pb isotope growth curve for the mantle (Fig. 16 ii), suggesting that the Takla Group basalt assimilated Pb from the upper crust. Assimilation of Asitka Group limestone by Takla Group basalt might account for their overlapping Pb isotope signatures. The more radiogenic signature for the Sofia basalt sample (Fig. 16 ii) might be the result of potassic alteration associated with the nearby granodiorite. Toodoggone Formation rocks commonly have Pb isotope values that are more radiogenic than Takla and Asitka Group rocks. The Toodoggone Formation data closely overlap the range of Pb isotope values for plutonic rocks in the district (Fig. 16 ii), which suggests that their respective magmas were derived from a common magma chamber and/or that they assimilated similar country rocks during their emplacement.

Plutonic rocks

Lead isotope values for the plutons are more radiogenic than the average Pb isotope signature of the mantle, suggesting that the plutons assimilated Pb from the upper crust (Fig. 17 i and ii). More specifically, all but the Mex, Pine, and Fin plutons, have Pb isotope values that overlap values for Toodoggone Formation rocks. Some plutons display Pb isotope values that are comparable with values for Asitka Group limestone and Takla Group volcanic country rocks (Fig. 17 iii), suggesting the plutons assimilated country rocks during their emplacement.

Lead isotope data for the Maple Leaf granodiorite, which hosts the Kemess South ore body, plot in two main groups: a loosely grouped radiogenic data set and a second, less radiogenic group of two analyses that demonstrate overlapping error envelopes (Fig. 17 i). The more radiogenic data represent plagioclase and alkali feldspar separates from the granodiorite that are heterogeneously altered by hydrothermal/meteoric fluids; they may also be contaminated by micro-inclusions of U- and Th-bearing minerals such as zircon. The least-radiogenic Pb isotope values for the mineralized granodiorite at Kemess South are similar to values for the nearby diorite host to the Kemess North ore body, indicating that they might

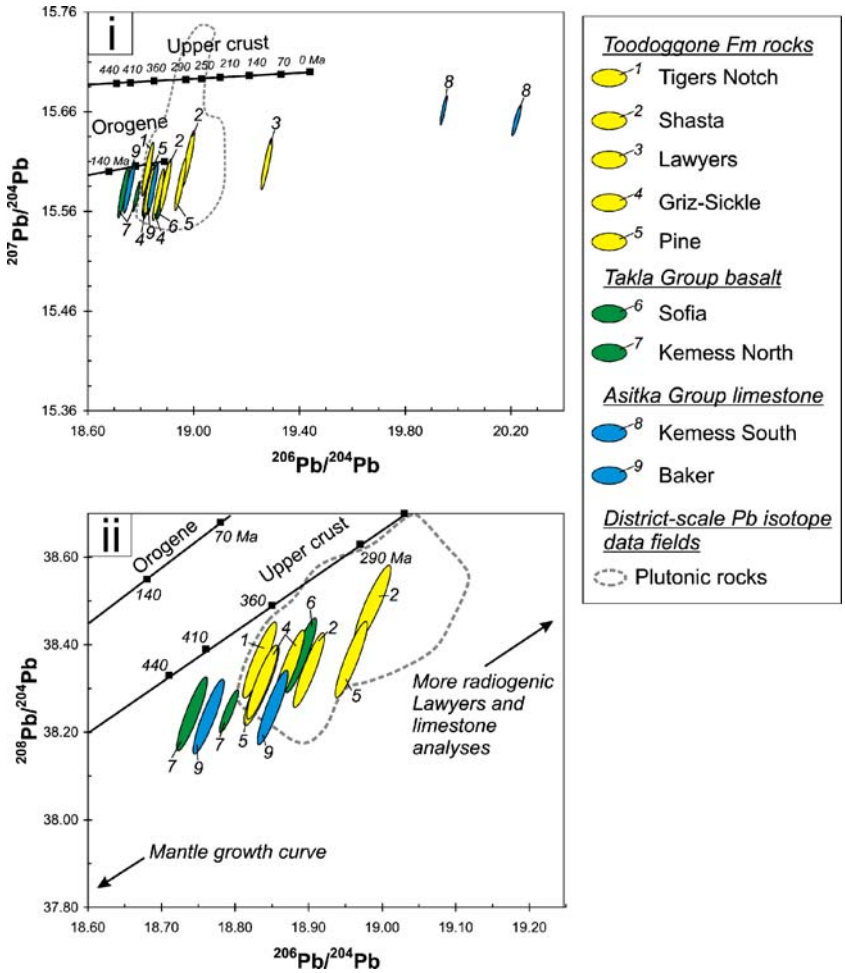

Fig. 16 The plots show Pb isotope values for calcite, plagioclase, and alkali feldspar separates from Asitka Group limestone, Takla Group basalt, and Toodoggone Formation andesitic rocks in the district. Also shown is the Pb isotope field for plagioclase and alkali feldspar separates from least-altered plutons (based on data presented in Fig. 17). Data from Kemess North and Pine are from McKinley (2006) and Dickinson (2006), respectively. The upper crust and orogene growth curves of Zartman and Doe (1981) are included for reference. *i* The uranogenic diagram shows all country rock Pb analyses, including radiogenic limestone samples from Kemess South and Toodoggone Formation rocks from Lawyers. *ii* The thorogenic diagram shows country rock data with the exception of the more radiogenic samples

share a common deeper magmatic source and/or interacted with compositionally similar country rocks prior to their emplacement.

The Pine quartz monzonite and Mex monzonite are more radiogenic than most other plutons in the district (Fig. 17 i and ii), whereas the nearby ca. 218 Ma Fin pluton has overlapping values with several ca. 202 to 197 Ma mineralized and barren plutons despite their ~16 m.y. difference in age. Hence, Pb isotope data for plutons in the district are broadly similar regardless of differences in their emplacement ages, metal enrichment, and geographic distribution. These similarities probably highlight the influence of country rock assimilation in controlling the final Pb isotope signature of plutons.

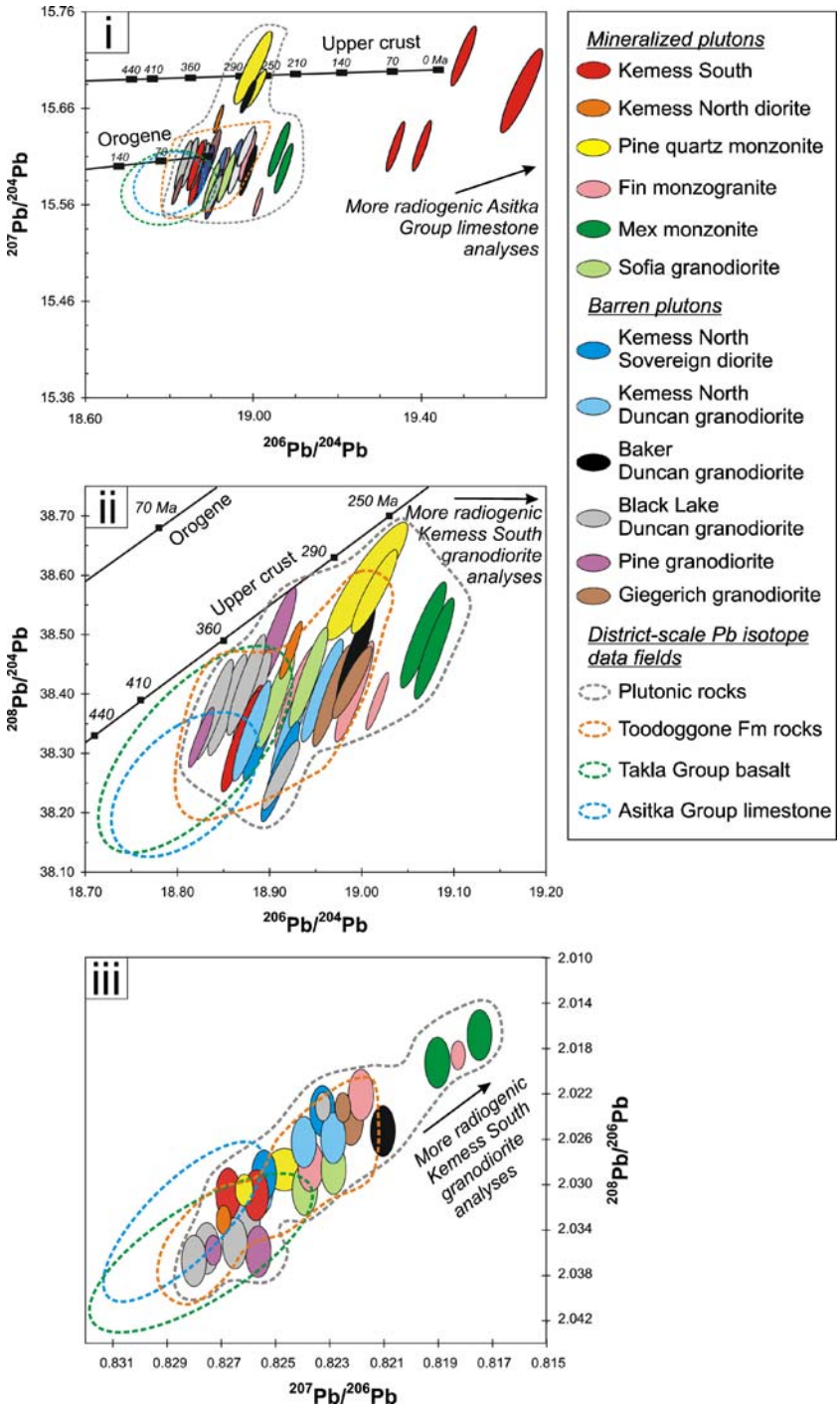

Fig. 17 Lead isotope data are displayed for plagioclase and alkali feldspar separates from mineralized and barren plutonic rocks in the Toodoggone district. Also shown for reference are Pb isotope fields for Asitka Group limestone, Takla Group basalt, and Toodoggone Formation andesitic rocks in the district (based on data presented in Fig. 16). Kemess North data are from McKinley (2006), whereas Pine and Fin data are from Dickinson (2006). The upper crust and orogene growth curves of Zartman and Doe (1981) are included for reference. *i* The uranogenic diagram shows all plutonic Pb isotope analyses, including radiogenic granodiorite samples from Kemess South. *ii* The thorogenic diagram shows an enlarged area of the Pb isotope plot and demonstrates that the mineralized and barren plutons are indistinguishable based on their Pb isotope ratios. *iii* The $^{207}Pb/^{206}Pb$ versus $^{208}Pb/^{206}Pb$ diagram demonstrates that the Kemess South, Kemess North, and Pine plutons have overlapping Pb isotope ratios. Fin data are variable, whereas Mex data are different from all other plutons in the district

Sulfide minerals from porphyry and low-sulfidation epithermal veins

Sulfide minerals from porphyry Cu–Au±Mo and epithermal Au±Ag veins have Pb isotope values that are more radiogenic than the mantle or lower crust. The data broadly overlap the ranges for district examples of Asitka Group limestone, Takla Group basalt, Toodoggone Formation rocks, and plutonic rocks (Fig. 18 i and ii). Lead isotope ratios for early- to post-mineralization-stage veins at Kemess South and Kemess North overlap and display comparable trends. For example, in both deposits, early-stage veins associated with potassic alteration mineral assemblages display the tightest overlap with Pb isotope

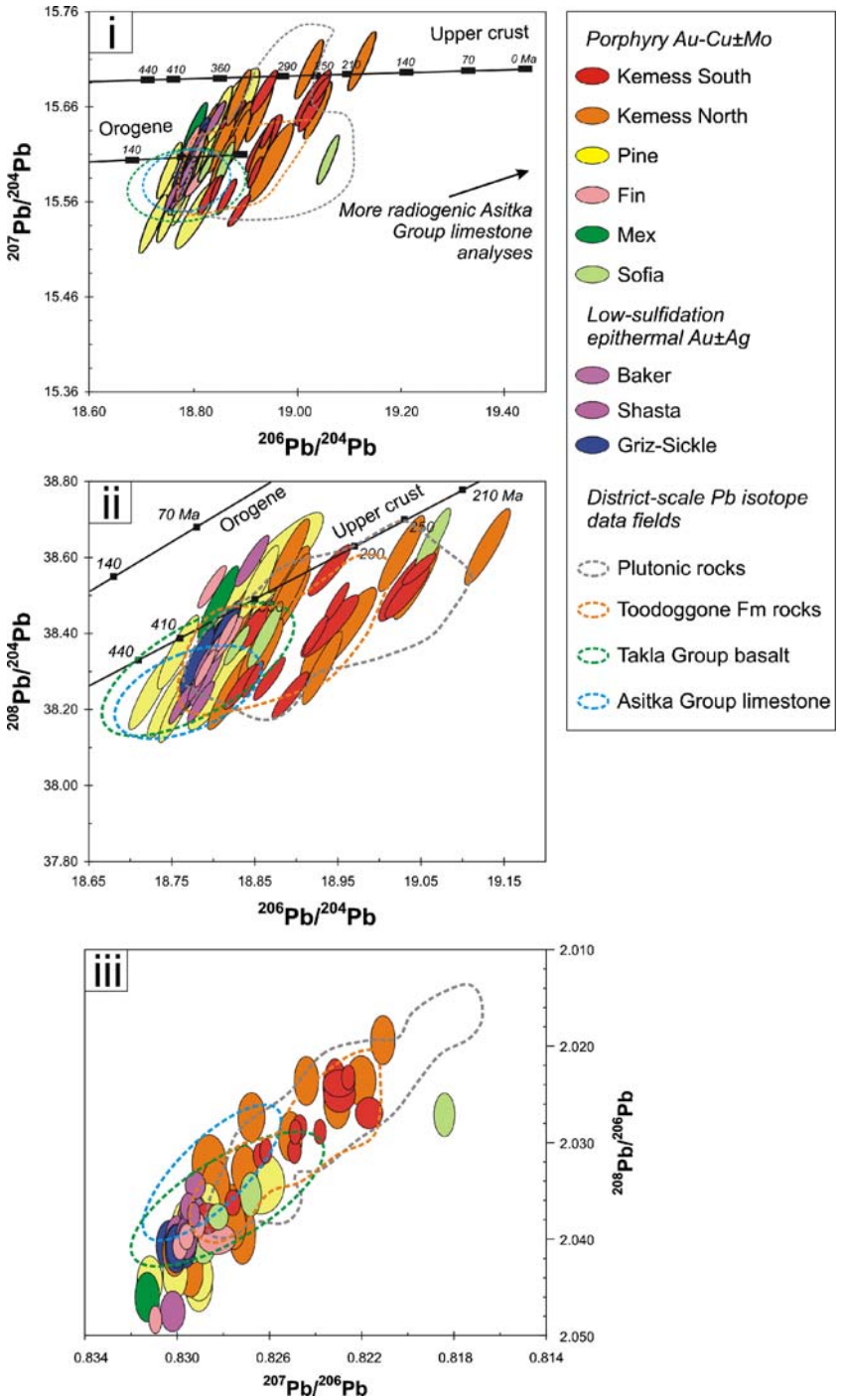

Fig. 18 Lead isotope data are shown for pyrite, chalcopyrite, sphalerite, and galena separates from porphyry Cu–Au±Mo and low-sulfidation epithermal Au±Ag occurrences in the Toodoggone district. Also shown for reference are Pb isotope fields for country rocks and plutonic rocks in the district. Kemess North data are from McKinley (2006), whereas Pine and Fin data are from Dickinson (2006). The upper crust and orogene growth curves of Zartman and Doe (1981) are included for reference. *i* The uranogenic diagram demonstrates that sulfides associated with Early to Post-mineralization-stage veins at Kemess South and Kemess North, and fault-hosted Cu–Au veins at Sofia, are comparable. *ii* The thorogenic diagram demonstrates that Kemess South, Kemess North, and Sofia Pb isotope ratios are different to Pine, Fine, and Mex data. The latter group are more like low-sulfidation epithermal systems. One analysis from Sofia is significantly more radiogenic than other Sofia data and might be the result of contamination by micro-inclusions of U- and Th-bearing minerals. *iii* The $^{207}Pb/^{206}Pb$ versus $^{208}Pb/^{206}Pb$ diagram indicates that Pb isotope data for sulfide minerals from Kemess South and Kemess North are most like their host intrusions. In contrast, Pb isotope data for sulfide minerals from the remaining porphyry systems and low-sulfidation epithermal systems are more comparable with the Pb isotope signatures of Asitka and Takla Group country rocks

values for their respective host plutons (McKinley 2006). The correlation between their Pb isotope values suggests that fluids and metals at Kemess South and Kemess North originated from the same deep magma chamber that generated the plutons. In comparison, Pb isotope values for main- and late-stage veins at both deposits have a greater spread than early-stage vein. The values overlap data for the respective plutonic hosts but also values for district-scale Takla and Asitka Group country rock. These relationships suggest that the fluids and metals associated with the main- to late-stage veins had a magmatic origin but interacted with nearby country rock prior to mineral deposition.

No sulfide minerals from main-stage veins at Pine were analyzed due to the low abundance of sulfide minerals (Dickinson 2006); however, Pb isotope data from late-stage veins overlap least-radiogenic values for sulfide minerals from main-stage veins at Kemess South and Kemess North (Fig. 18 iii). The Pine data also overlap main-stage veins from Fin and Mex, despite Fin being ~19 m.y. older than Pine. The comparable Pb isotope signatures shared by Pine and Fin sulfide minerals are most likely the result of the respective ore fluids or their plutons interacting with similar country rocks.

Low-sulfidation epithermal Au±Ag veins at Shasta, Baker, and Griz-Sickle have Pb isotope ratios for sulfide minerals that overlap Asitka and Takla Group country rocks. At Baker, the mineralized veins display Pb isotope values for pyrite that compare more closely with the values for nearby marbleized Asitka Group limestone than with granodiorite that crops out 200 m to the east of the A and B veins (Fig. 19 i). Similarly, at Shasta, Ag–Au veins from the JM and Creek zones have Pb isotope values (Fig. 19 ii) that are more similar to district values for Asitka and Takla Group rocks than their immediate Toodoggone Formation host rocks. Hence, Pb isotope data for low-sulfidation epithermal ore fluids record more fluid interaction with deep Asitka and Takla Group country rocks rather than nearby plutons or their immediate Toodoggone Formation host rocks.

Discussion

Comparison of porphyry Cu–Au±Mo systems and barren plutons in the Toodoggone district

Distribution, chemistry, and age of the plutons

Felsic igneous rocks that host porphyry-style Cu–Au±Mo mineralization include the Kemess South, Kemess North, Pine, Fin, Mex, Brenda, and Sofia intrusions, whereas plutons that have below background concentrations of metals include the Duncan, Giegerich, and the Sovereign plutons. All plutons intrude Asitka and Takla Group basement rocks, and rarely, the lowest member of the Toodoggone Formation (i.e., ca. 201 Ma Duncan Member rocks). Toodoggone Formation rocks straddle the andesite to andesite/basalt compositional fields of Winchester and Floyd (1977), whereas Takla Group rocks are mostly subalkaline basalt in composition (Fig. 20 i).

Porphyry Cu–Au±Mo systems are genetically associated with small-volume (<1 km^3) igneous stocks or dikes that are up to 44 km apart (i.e., between Kemess South and Sofia), with deposit clustering occurring only at Pine–Fin–Mex. Although the barren plutons have a similar spatial distribution to the mineralized plutons, the barren plutons have exposed surface areas that are several orders of magnitude greater than mineralized plutons (e.g., the Duncan pluton; Fig. 1). Mineralized plutons are texturally homogeneous and do not display any systematic variation in texture with depth or lateral distance from porphyry centers. The plutonic hosts are porphyritic with 20 to 50 vol.% phenocrysts of plagioclase, hornblende, biotite, quartz, and alkali feldspar. The Kemess South and Kemess North plutons have closely packed phenocrysts of plagioclase and alkali feldspar surrounded by an aphanitic groundmass. Barren plutons, such as the Duncan and Giegerich plutons, have the same primary igneous mineral assemblage as mineralized plutons but are equigranular.

Chemical compositions of least-altered porphyry intrusions range from tonalite to granodiorite, with barren intrusions being tonalite and most of the mineralized intrusions granodiorite (Fig. 20 ii). Potassic alteration of plagioclase (i.e., a loss of Ca and addition of K) shifts some mineralized porphyry compositions to the left and/or downwards on Fig. 20 ii (e.g., Pine quartz monzonite). Barren plutons in the district are mostly metaluminous (Fig. 20 iii), whereas mineralized plutons are more likely to straddle the metaluminous and peraluminous fields of the Maniar and Piccoli (1989) classification diagram. The highly peraluminous nature of some intensely altered Kemess South and Kemess North plutons might be caused by the high mobility of Ca, Na, and K in these altered rocks. All plutons belong to the high-K calc-alkaline granitoid series, with compositions that are comparable with volcanic-arc granites (Fig. 20 iv and v). The igneous equilibrium mineral assemblage quartz–magnetite–titanite in least-altered samples of all plutons places the magmas above the quartz–magnetite–fayalite buffer, indicating that they were oxidized at the time of crystallization. All plutons are enriched in light rare earth elements relative to heavy rare earth elements (REE); none show a negative Eu anomaly. Mineralized plutons at Pine, Kemess South, Kemess North, Sofia, and Mex have comparable REE trends, with the closest geochemical affiliation existing between the Kemess South and Kemess North plutons. The

Fin monzogranite displays anomalously low REE (e.g., La and Yb; Fig. 20 vi). In all porphyry systems, Cu, followed by Au and Mo, are the main economic metals in terms of volume. Zinc, Pb, and Ag are commonly present in uneconomic concentrations, associated with centimeter-wide, quartz–calcite veins located distal to intrusions (e.g., at Kemess South; Rebagliati et al. 1995). The Fin monzogranite is unusual in that it is Cu–Au-poor but enriched in Mo, Zn, and Pb (Dickinson 2006).

Emplacement ages of plutons in the district display a bimodal distribution, with the Fin pluton emplaced about 16 m.y. before the more volumetrically dominant, ca. 202 to 191 Ma plutonic suite (Fig. 21). The onset of district-scale plutonism at ca. 202 Ma coincided with the formation of the largest porphyry Cu–Au±Mo systems in the district (e.g., Kemess North, Kemess South). With the exception of the Pine pluton, which hosts mineralization that formed as late as ca. 194 Ma, the later-forming (i.e., 197 to 191 Ma) plutons are mostly unmineralized. Metals were either not present in these magmas in significant concentrations or magmatic–hydrothermal processes were not conducive for metal concentration.

Vein histories and hydrothermal alteration in porphyry Cu–Au±Mo systems

The Kemess South, Kemess North, and Pine plutons display comparable vein paragenetic sequences that include

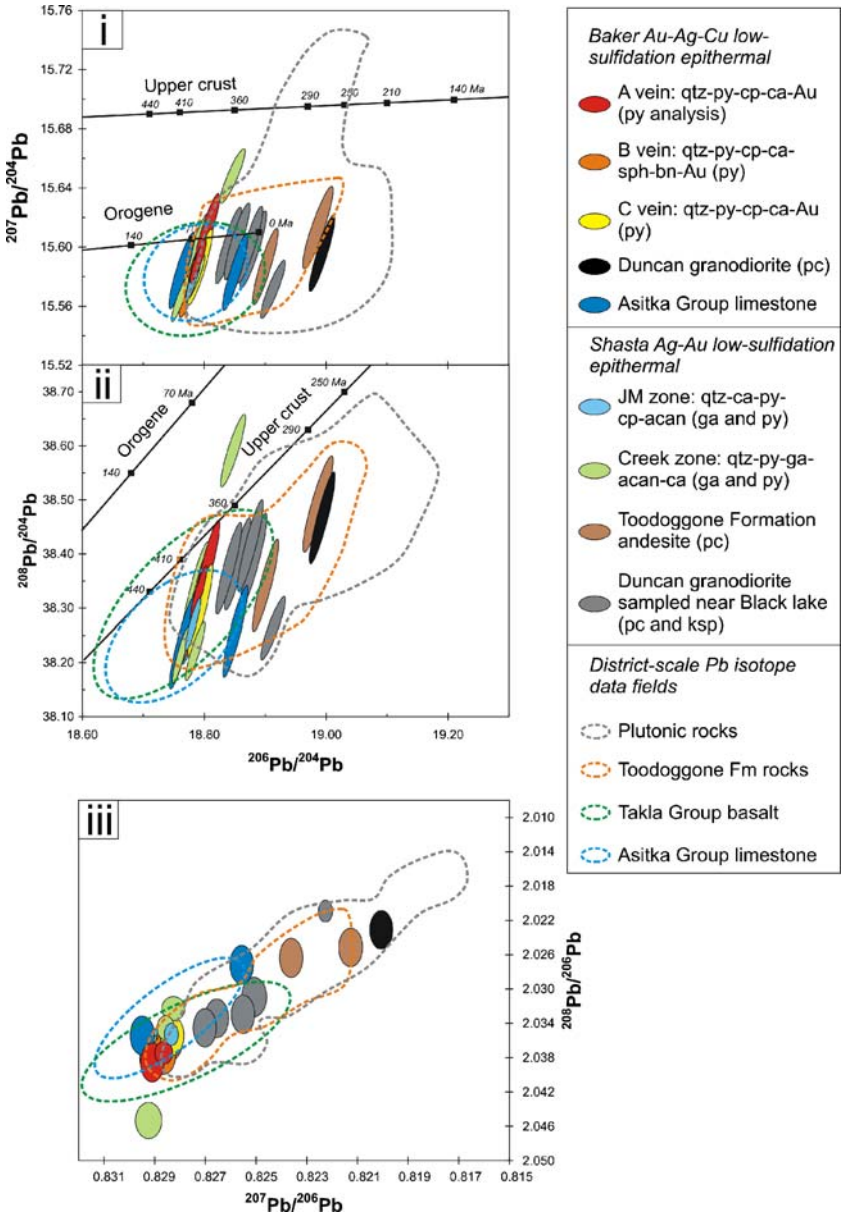

Fig. 19 Lead isotope data are presented for feldspar and sulfide mineral separates from the Baker and Shasta low-sulfidation epithermal deposits. Also shown for reference are Pb isotope fields for country rocks and plutonic rocks in the district. The upper crust and orogene growth curves of Zartman and Doe (1981) are included for reference. The uranogenic (*i*), thorogenic (*ii*), and $^{207}Pb/^{206}Pb$ versus $^{208}Pb/^{206}Pb$ (*iii*) diagrams demonstrate that Pb in the ore fluids at Baker most likely reflects the equilibration between the ore fluids and Asitka and Takla Group country rocks before metal deposition. Similarly, Pb isotopes for sulfide minerals at Shasta show greater similarity to Asitka and Takla Group rocks, rather than nearby plutons or the immediate Toodoggone Formation host rocks to mineralization. Abbreviations: *acan* acanthite, *bn* bornite, *ca* calcite, *cp* chalcopyrite, *ga* galena, *ksp* alkali feldspar, *pc* plagioclase, *py* pyrite, *qtz* quartz

up to ten cross-cutting vein stages, which are divided into early-, main-, late-, and post-mineralization-stage veins. The comparatively poorly mineralized Fin, Mex, Brenda, and Sofia intrusions do not exhibit the same number of vein stages or the same intensity of vein occurrences compared with the well-mineralized plutons. The differences suggest that the better mineralized systems were longer-lived, more complex, and/or experienced greater fluid flux.

In all mineralized plutons, the early-stage fluid event is characterized by (a) magnetite-rich±biotite±chalcopyrite veins with alkali feldspar alteration envelopes (e.g., Kemess North, Pine, Sofia), (b) sugary-textured, quartz–biotite-rich–alkali feldspar–magnetite–chalcopyrite veins (e.g., stage 1 veins at Kemess South), and (c) banded, quartz-rich–pyrite–chalcopyrite–magnetite–molybdenite–gold veins (e.g., Stage 2 veins at Kemess South, Kemess North, Pine, Sofia). The latter two styles of early-stage veins are comparable with the El Salvador "A" and "B" veins described by Gustafson and Hunt (1975). Main-stage veins are dominated by pyrite, quartz, chlorite, sericite, and

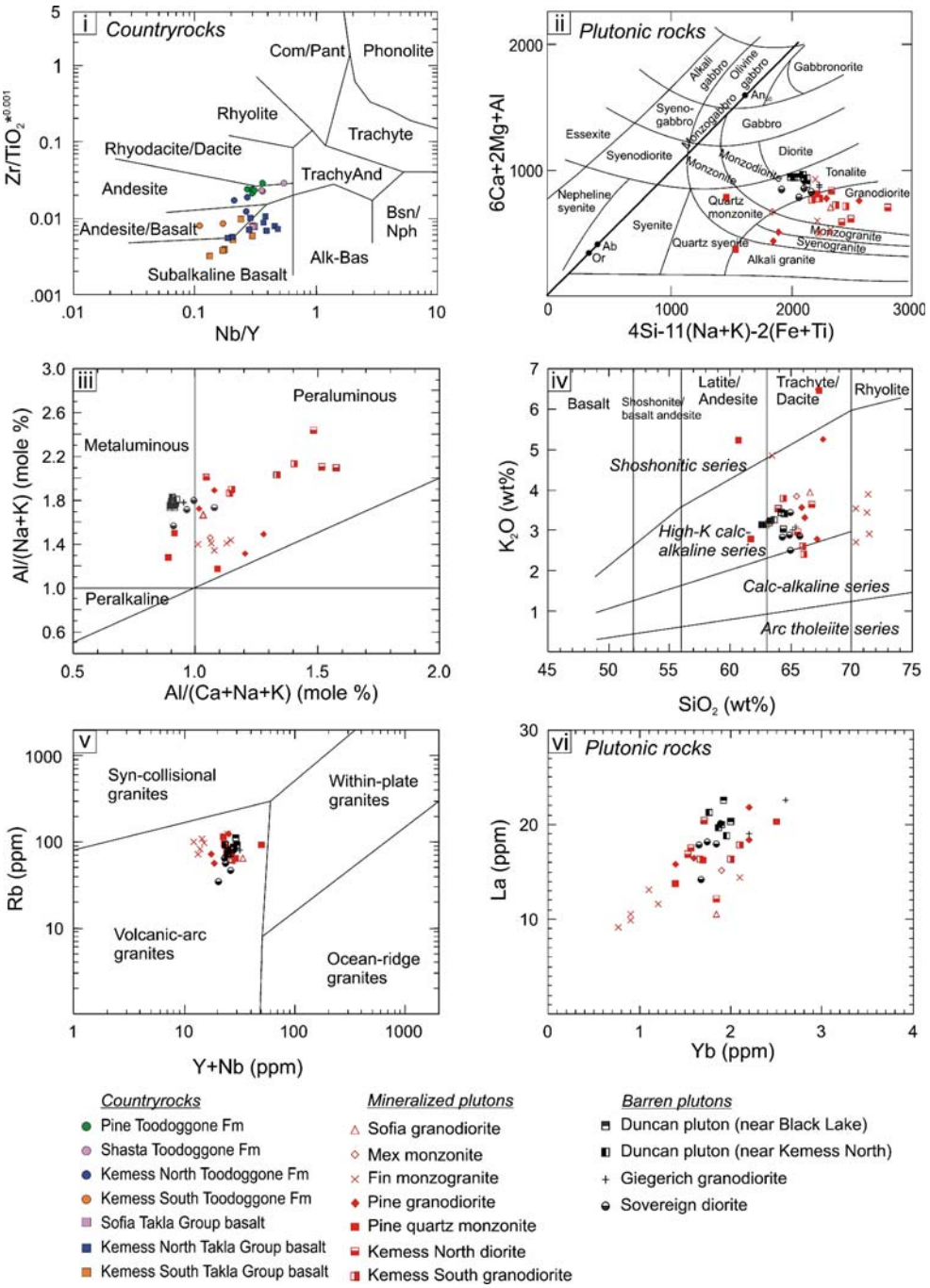

Fig. 20 Discrimination diagrams compare the composition of representative least-altered country rocks and plutonic rocks in the Toodoggone district: *i* Toodoggone Formation rocks straddle the andesite to andesite/basalt compositional fields of Winchester and Floyd (1977), whereas Takla Group rocks are mostly subalkaline basalt in composition. *ii* Most plutonic rocks span the tonalite–granodiorite–monzogranite fields of the De la Roche et al. (1980) classification diagram. The Pine pluton displays the greatest spread in composition due to the variable intensity of hypogene alteration. *iii* Plutons are mostly metaluminous based on the Maniar and Piccoli (1989) discrimination diagram; some data overlap the peraluminous field as a result of intense hypogene alteration in these samples. *iv* Plutons belong to the high-K, calc-alkaline granitoid series as defined by Peccerillo and Taylor (1976); note the spread in the variably altered Pine quartz monzonite data and the more SiO_2-rich nature of the older Fin monzogranite. *v* All plutons in the district are considered to have chemistries that are comparable with volcanic-arc granites (Pearce et al. 1984). *vi* Mineralized and barren plutons display significant overlap in their immobile element ratios. The Fin pluton shows the greatest compositional difference from other plutons. Kemess North data are from McKinley (2006), whereas Pine, Fin, and Mex data are from Dickinson (2006)

calcite, with a diverse range of metallic minerals, including chalcopyrite, molybdenite, bismuthinite, pyrrhotite, and gold (e.g., stage 3 veins at Kemess South, Kemess North, Sofia). These main-stage veins are associated with quartz–pyrite±sericite (phyllic) or chlorite–quartz–pyrite–illite± chalcopyrite±molybdenite (intermediate argillic) alteration assemblages. Epidote–pyrite–chalcopyrite–molybdenite main-stage veins at Fin (Dickinson 2006) are anomalous in the district in that they probably represent sodic (±calcic) alteration rather than distal propylitic alteration associated with the nearby Pine porphyry system. Late-stage veins comprise mostly pyrite with minor quartz, chalcopyrite, sericite, chlorite, calcite, and hematite (e.g., stage 4 veins at Kemess South and Kemess North). At Pine, late-stage veins

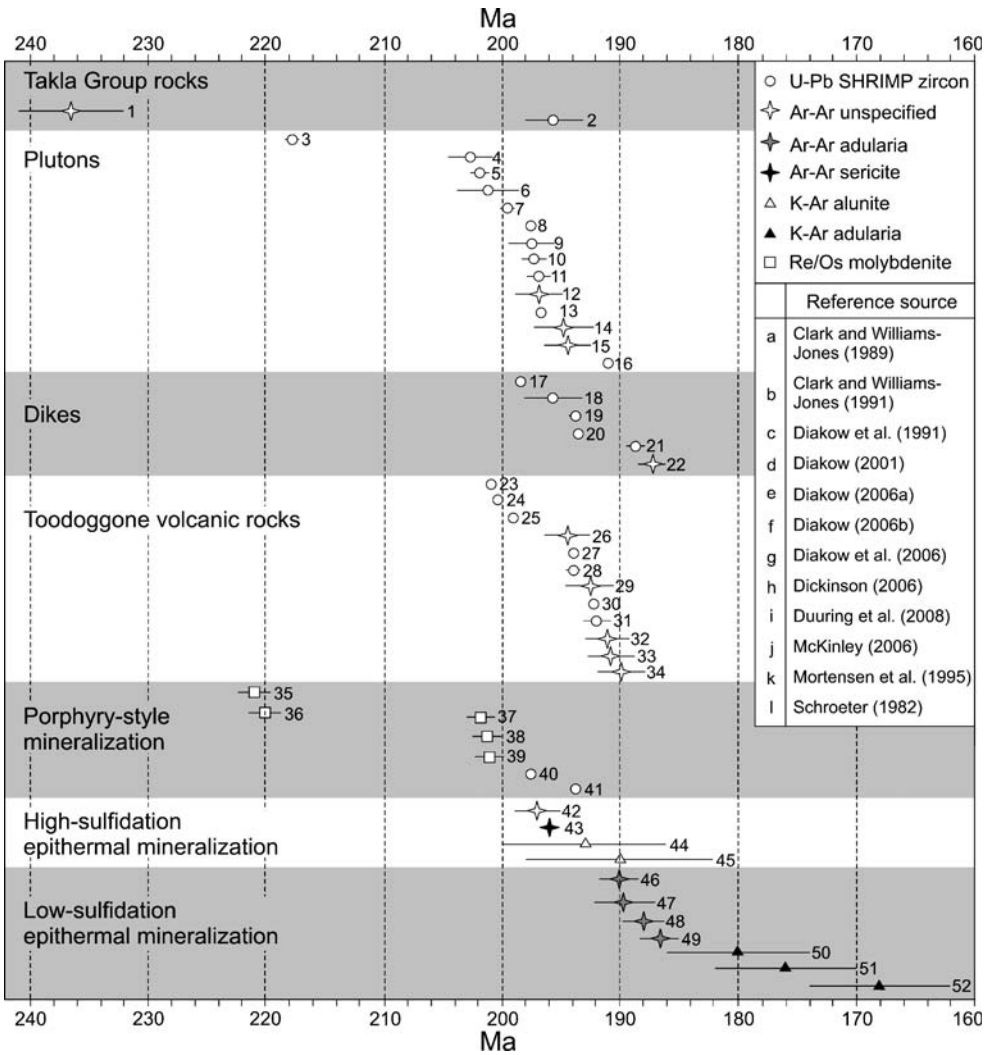

Fig. 21 Summary of geochronological data for the Toodoggone district. The *solid horizontal lines* represent the 2σ error values for the analyses. Data include: *1*, a granitic clast in Takla Group conglomerate[d]; *2*, Takla Group volcanic rock[d]; *3*, Fin monzogranite[h]; *4*, Sovereign diorite[d]; *5*, Kemess North diorite[f]; *6*, Black Lake Jensen pluton[d]; *7*, Kemess South Maple Leaf pluton[k]; *8*, Pine quartz monzonite[h]; *9*, Giegerich granodiorite[d]; *10*, Duncan granodiorite[d]; *11*, Black Lake monzonite[e]; *12*, Duncan granodiorite[e]; *13*, Jock Creek pluton[e]; *14*, Black Lake granodiorite[e]; *15*, Black Lake granodiorite[e]; *16*, Fredrikson pluton[d]; *17*, Monzonite dike[e]; *18*, Quartz rhyolite dike[d]; *19*, stage 1 syenite dike at Pine[h]; *20*, Pine rhyolite dike[h]; *21*, Griz-Sickle dacite dike[e]; *22*, Brenda dikes[e]; *23*, Duncan Member andesite tuff[h]; *24*, Duncan Member dacite tuff[d]; *25*, Duncan Member lapilli tuff[d]; *26*, Duncan Member lapilli tuff[d]; *27*, Saunders Member[d]; *28*, Saunders Member[d]; *29*, Saunders Member[d]; *30*, Graves Member[e]; *31*, Junkers Member[e]; *32*, Kemess Member[d]; *33*, Kemess Member[d]; *34*, Kemess Member[d]; *35*, Fin molybdenite[h]; *36*, second Fin molybdenite[h]; *37*, Kemess North molybdenite[j]; *38*, Kemess South molybdenite in Takla Group basalt[i]; *39*, Kemess South molybdenite in granodiorite[i]; *40*, Pine quartz monzonite[h]; *41*, Pine Cu-bearing syenite dike[h]; *42*, Alunite ridge[g]; *43*, Bonanza deposit[b] (no error values were reported); *44*, Jan prospect quartz–alunite–dickite alteration[a]; *45*, Al deposit[l]; *46*, Griz-Sickle[g]; *47*, Cliff Creek deposit[b]; *48*, Lawyers Amethyst Gold Breccia zone[b]; *49*, Shasta deposit[b]; *50*, Lawyers Amethyst Gold Breccia zone[c]; *51*, Golden Lion prospect[c]; *52*, Metsantan prospect[c]

also include anhydrite–pyrite veins. These veins are comparable with the "D" veins of Gustafson and Hunt (1975). Post-mineralization-stage veins, including anhydrite–pyrite, anhydrite–gypsum, calcite–zeolite, and chlorite veins are common at Kemess South, Kemess North, Pine, and Fin.

Early-stage potassic alteration zones are well preserved at Pine and Sofia but are poorly preserved at Kemess South and Kemess North due to the pervasive replacement by phyllic and intermediate argillic alteration. Epidote–chlorite–carbonate (propylitic alteration) assemblages occur at Kemess South, Kemess North, and Pine in areas distal to the mineralized pluton. Supergene alteration is well defined at Kemess South and Kemess North but is not as pronounced at the other porphyry occurrences. Kemess South is the only porphyry system that contains economic concentrations of remobilized Cu in exotic positions relative to the porphyry host. Gypsum–anhydrite transition lines occur within 75 m of the present surface at Kemess North and Pine but are less obvious at Kemess South. They occur where surface meteoric water has hydrated hypogene anhydrite to secondary gypsum, resulting in an increase in rock volume and permeability.

Conditions of ore deposition and the source of metals in ore fluids

The absence of hydrothermal breccias in any of the Toodoggone district porphyry deposits, suggests that, although hydrostatic fluid pressures intermittently exceeded lithostatic pressures to form hydraulic fractures and veins, it did not do so with sufficient force to produce breccias. Microthermometric studies at Kemess South and Kemess North do not accurately constrain the conditions controlling metal deposition; however, a progressive decline in the temperature of early-stage fluids to late-stage hydrothermal fluids is demonstrated by the transition from potassic to phyllic alteration mineral assemblages, and most likely contributed to the saturation of metals in the fluids and deposition of metals. At the same time, the transition from lithostatic to hydrostatic pressures in the plutons and proximal country rock probably resulted in widespread hydraulic fracturing and vein formation.

Hydrothermal alteration mineral assemblages, as well as S, C, O, and Pb isotope values for the ore fluids, reflect interactions between the magmatic–hydrothermal fluid and the wallrock. Country rock Pb, C, and perhaps metals, were also added to main-stage to post-mineralization-stage fluids at Kemess South, Kemess North, and Pine due to the interaction between the magmatic fluids, Asitka and Takla Group country rocks, and also cooler low-salinity meteoric fluids and/or metamorphic fluids.

In summary, the similar chemistry and emplacement ages (202 to 197 Ma) for the Kemess South, Kemess North, and Pine plutons probably reflects their contemporaneous genesis from a common magma source located more than 2 km below the paleosurface. Given that the Duncan pluton is presently exposed for a strike distance of more than 35 km along the western margin of the district (Fig. 1), it is feasible that a magma chamber with a 30 to 50 km^2 surface area could have underlain the mineralized porphyry occurrences in the district. Mineralized plutons and dikes were probably episodically emplaced during a 5 to 7 m.y. interval. Local tectonic conditions triggered and controlled emplacement of plutons, apophyses, and dikes into structures in dominantly Asitka and Takla Group country rocks. The assimilation of country rocks influenced the resultant chemistries of the evolving plutons as well as the composition of the magmatic–hydrothermal ore fluids, causing variable shifts from the initial Pb, C, and O isotope values for these fluids. Sulfur isotope values for early- to post-mineralization-stage veins overlap at Kemess South, Kemess North, Pine, and Fin (i.e., $\delta^{34}S_{pyrite}$ values range from −2‰ to 3‰; Fig. 14 i) and suggest a magmatic source for S in the ore fluids. However, partial remobilization of sulfide minerals by successive hydrothermal fluid events may have contributed to the overlap in $\delta^{34}S_{pyrite}$ values in the deposits. Injection of mafic magmas into the base of the silicic chamber to the porphyry deposits may have occurred during the felsic magmatism. Syn-mineral mafic intrusions exist at Pine and post-mineral gabbro dikes are common at Kemess South and Kemess North.

Genetic links between porphyry Au–Cu±Mo and epithermal Au±Ag systems

Available geochronological data for the district indicates that a close temporal overlap exists between porphyry intrusion ages (ca. 205 to 191 Ma) and porphyry-style mineralization ages (ca. 203 to 194 Ma) (Fig. 21), providing good supporting evidence for a genetic link between these events. High-sulfidation epithermal mineralization ages (ca. 201 to 182 Ma) overlap the crystallization ages of nearby porphyry intrusions (e.g., coeval high-sulfidation alteration and emplacement of the Jock Creek pluton at Griz-Sickle) and the youngest example of porphyry-style mineralization in the district (i.e., ca. 193.8±0.5 Ma porphyry Cu–Au mineralization at Pine). Based on these timing relationships, a genetic link most likely exists between high-sulfidation epithermal systems and porphyry intrusions in the district. In contrast, low-sulfidation epithermal mineralization ages (ca. 192 to 162 Ma) only overlap the poorest quality high-sulfidation epithermal mineralization ages (i.e., those with the largest errors) and do not overlap with any of the porphyry intrusion ages.

Low-sulfidation epithermal mineralization ages do, however, overlap the ages of some local dikes (ca. 199 to 187 Ma) and the youngest of the members of the Toodoggone Formation (Fig. 21). These relationships are good evidence that most low-sulfidation systems are not genetically related to the porphyry and high-sulfidation epithermal systems, although it is still possible that heat from cooling subvolcanic intrusions associated with the formation of the Toodoggone Formation (ca. 201 to 188 Ma) drove the hydrothermal convection of fluids that formed the low-sulfidation veins.

The Baker low-sulfidation epithermal deposit provides the best evidence for a genetic link between epithermal and magmatic ore fluids. Compared with the Shasta, Lawyers, and Griz-Sickle low-sulfidation epithermal occurrences, the Baker ore zones are Ag-poor (Ag/Au ratio of 9 compared with 30 to 200 at the other deposits) and the ore fluid was hotter (>468°C), more saline, and deposited its metals at depths of >2.0 km. These crustal conditions are also hotter and deeper than for most epithermal systems, which commonly have temperature and depth ranges of 150 to 300°C and 50 to 1,100 m, respectively (Simmons et al. 2005). Sulfur, C, O, and Pb isotope data support a magmatic fluid contribution as well as significant fluid interaction with nearby Asitka Group limestone and possibly Takla Group volcanic rocks prior to metal deposition. The exact source of magmatic fluids and metals is uncertain since the Pb isotope signature of the Baker ore fluid does not correspond to any examined pluton in the vicinity of the Baker deposit.

The Shasta, Lawyers, and Griz-Sickle low-sulfidation epithermal systems have no demonstrable genetic association with magmatic fluids. Instead, their fluid inclusion data indicate the involvement of low-temperature (175 to 335°C), low-salinity (1 to 11 equiv. wt.% NaCl) ore fluids that deposited metals at depths of <850 m. Their corresponding C, O, H, S, and Pb isotope data suggest the prevalence of meteoric and/or metamorphic ore fluids that interacted with Asitka Group limestone and Takla Group volcanic rocks, and locally with organic C-rich epiclastic Toodoggone Formation rocks (e.g., at Lawyers) prior to metal deposition. Fluid boiling, cooling, and fluid interaction with wallrocks are probable mechanisms for metal deposition.

High-sulfidation epithermal systems in the district require further evaluation since the Griz-Sickle and Silver Pond systems lacked veins and sulfide minerals, so were not conducive for fluid inclusion or S and Pb isotope studies. However, low-temperature (i.e., 180 to 200°C) and low-salinity (i.e., <3 equiv. wt.% NaCl) fluids responsible for Au-bearing veins at the high-sulfidation Al deposit (Clark and Williams-Jones 1986) do not support the involvement of magmatic fluids.

High- and low-sulfidation epithermal systems in the Toodoggone district probably reflect circulation of meteoric and/or metamorphic fluids through Asitka and Takla Group country rocks prior to metal deposition in overlying Toodoggone Formation rocks (e.g., Shasta, Lawyers, Griz-Sickle), or rarely, in Takla Group basalt (e.g., Baker). The involvement of porphyry intrusions in epithermal systems, in terms of contributing metals, fluids, or heat, can only be demonstrated at Baker. However, given the spatial and temporal coincidence between district-scale plutonism, volcanism, and epithermal mineralization, it is feasible that felsic magmatism caused the convection of meteoric/metamorphic fluids and possibly metals through country rocks even if there was no direct metal contribution from the magmas. Second- and third-order, kilometer-scale faults are oriented parallel, but internally, to the NW- and NE-trending margins of horst-and-graben style blocks. These were probably active before and during plutonism, and were subsequently reactivated during district-scale N–S-directed compression that coincided with epithermal mineralization (e.g., at Shasta). Consequently, these structures provided the main control on the location of low- and high-sulfidation epithermal deposits.

Implications for exploration in the Toodoggone district

Porphyry Cu–Au±Mo and epithermal Au±Ag systems remain as high-priority exploration targets in the district compared with rare placer Au occurrences and Au–Cu skarns. Skarns are mainly low-tonnage, low-grade occurrences that are restricted to chemically favorable Asitka Group limestone near plutons. Plutons emplaced at ca. 202 to 197 Ma host the largest porphyry-style deposits in the district and consequently represent more important exploration targets than poorly mineralized, later-forming plutons, such as the Duncan pluton. The Fin porphyry system represents a previously unrecognized, older plutonic and Cu–Au–Mo mineralization event in the district. The frequency and distribution of this plutonic suite are presently unknown and it is unclear if it deserves targeting. Geochronological dating of weakly Cu-mineralized syenite dikes in the Pine porphyry system now extends the porphyry-style mineralization event in the district to as late as 193.8±0.5 Ma (Dickinson 2006). This not only indicates a temporal coincidence between porphyry-style mineralization in the southern half of the district and epithermal deposits in the north, but also extends the range of possible host rocks to include the oldest member of the Toodoggone Formation (i.e., Duncan Member rocks).

In terms of vectors for porphyry systems, zoned alteration patterns in country rocks provide the biggest footprint for mineralization. At Kemess South, Kemess North, and Pine, the alteration footprints are two to five

times larger than the distribution of economic Au–Cu concentrations. Mobile elements, such as K, Na, and Ca, are good indicators of hydrothermal alteration and potential mineralization in plutons; however, immobile element ratios (e.g., La/Yb) in least-altered plutons do not discriminate barren from mineralized plutons within the ca. 202 to 191 Ma plutonic suite. Lead isotopes are unlikely to be useful in identifying mineralized plutons because the isotopic signatures of the plutons are commonly influenced by the country rocks that they pass through. Metal zonation, vein density, and the actual exposure of the mineralized pluton are other important indicators but they may not always be readily observable due to abundant glacial sediment surface cover in the district (e.g., at Sofia and Pine). Apart from drilling data, standard geophysical surveys that include resistivity, gravimetric, magnetic, radiometric, and induced polarization techniques, are useful for defining the distribution of plutons and alteration mineral assemblages beneath surface cover.

Pressure estimates from fluid inclusions in mineralized veins from Kemess South and Kemess North indicate that porphyry-style mineralization occurred at crustal depths greater than 2 km. The prevalence of these deposits in Asitka and Takla Group basement rocks exposed in the southern half of the district suggests that erosion and uplift rates were greater in this area. In contrast, the northern half of the district mostly contains Toodoggone Formation rocks and shallower (<850 m) epithermal systems. Any porphyry systems that might exist in the northern half of the district are likely to be deeply buried beneath Toodoggone Formation units or be present within Asitka and Takla Group basement rocks that are exposed along the margins of the Toodoggone volcanic depression (e.g., near Sofia and Baker; Fig. 1).

The best vectors for low-sulfidation epithermal mineralization are the presence of hydrothermal alteration zonation, mineralized faults, and veins. All studied deposits display mappable potassic or phyllic centers, surrounded by phyllic or argillic alteration zones that grade into distal propylitic alteration zones. The ore zones are hosted by kilometer-scale, NW- and ENE-trending, steep-dipping faults. Conjugate mineralized faults (e.g., at Shasta) and dilational jogs are favorable sites for fluid focusing and coincide with wider orebodies. Regional geophysical surveys completed in the district to date did not accurately define hydrothermal alteration zones associated with low-sulfidation epithermal-style mineralization because the size of the systems (<1 km in strike length, <300 m wide) is below the resolution of the surveys. Surface mapping in combination with detailed geophysical surveys has been more successful in defining the extent and geometry of exposed or partly hidden orebodies.

Conclusions

Porphyry Cu–Au±Mo systems in the Toodoggone district are hosted by ca. 202 to 197 Ma, small-volume (<1 km^3), single-phase, porphyritic igneous stocks or dikes that are high-K calc-alkaline and have compositions comparable to volcanic-arc granites. The mineralized plutons and dikes intrude the oldest exposed rocks in the district, including the Asitka Group, Takla Group, and rarely, Duncan Member rocks of the Toodoggone Formation. Mineralized veins in the porphyry Cu–Au±Mo systems have S, C, O, and Pb isotope values that indicate that the ore fluids were sourced from a magma but interacted with Asitka and Takla Group country rocks before metal deposition. The 217.8±0.6 Ma Fin porphyry system is anomalous in that the pluton has a different age and chemistry than all other known porphyry Cu–Au±Mo occurrences in the district. Barren plutons have similar immobile element ratios and Pb isotope signatures as well as overlapping emplacement ages and geographic distribution to the mineralized plutons. They differ in that they are mostly equigranular and have larger exposed surface areas than mineralized plutons.

Low- and high-sulfidation epithermal systems are located in the northern half of the Toodoggone district study area. They are associated with second- and third-order faults that cut Toodoggone Formation rocks, or rarely, Takla Group basalt. Most known epithermal systems are situated within 2 km of exposed unmineralized plutons. High-sulfidation epithermal systems formed at ca. 201 to 182 Ma and coincide with the timing of district-scale plutonism and porphyry Cu–Au±Mo mineralization, whereas low-sulfidation systems formed later at ca. 192 to 162 Ma, coinciding with the emplacement of felsic dikes and Toodoggone Formation volcanism. The Baker low-sulfidation deposit is the only epithermal system that displays evidence for the involvement of a magmatic fluid. The Baker ore fluid was hot (>468°C), saline, and deposited its metals at depths of >2.0 km. Sulfur, C, O, and Pb isotope data support a magmatic contribution for ore fluids and possibly metals, and indicate significant fluid interaction with nearby Asitka and Takla Group country rocks. In contrast, the Shasta, Lawyers, and Griz-Sickle low-sulfidation epithermal deposits have fluid inclusion data that indicate the involvement of low-temperature (175 to 335°C), low-salinity (1 to 11 equiv. wt.% NaCl) ore fluids that deposited metals at much shallower depths of <850 m. Their corresponding C, O, H, S, and Pb isotope data suggest the prevalence of meteoric and/or metamorphic ore fluids that interacted with Asitka and Takla Group country rocks, and locally with organic C-rich epiclastic Toodoggone Formation rocks prior to metal deposition.

Porphyry and epithermal systems are the most important exploration targets in the Toodoggone district because of their

high-tonnage or high-grade potential, respectively. Porphyry systems hosted by Asitka and Takla Group basement rocks are most common in the southern half of the district due to higher rates of uplift and erosion in these areas. In contrast, shallow-forming epithermal systems are more common in younger Toodoggone Formation rocks in the northern half of the district. Plutons that were emplaced at ca. 202 to 197 Ma host the most economically significant porphyry-style deposits in the district and, therefore, represent more prospective targets than later-forming plutons. The Fin porphyry occurrence represents a previously unrecognized, older plutonic and Cu–Au–Mo mineralization event in the district and its economic significance is presently unknown.

Acknowledgements The present study is part of a NSERC–CRD grant funded research project between the University of British Columbia, Northgate Minerals Ltd., and Stealth Minerals Ltd. The latter two companies are thanked for providing generous financial and logistical support for fieldwork in the Toodoggone district. Northgate Minerals Ltd. mining and exploration staff, including Carl Edmunds, Brian Kay, Ron Konst, Brian O'Connor, Gary Parrup, and Chris Rockingham, provided logistical support as well as access to Kemess South, Kemess North, and diamond drill core. Stealth Minerals Ltd. staff, including Dave Kuran and Bill McWilliam, provided generous support during fieldwork and access to Pine, Fin, Mex, Griz-Sickle, and Sofia. Mel Rahal from Sable Resources is thanked for providing access to the Baker pits and drill core. Field assistants, Andy Orr and Colin Smith, contributed greatly with their enthusiasm and dedication during fieldwork and later laboratory work. Richard Friedman and Janet Gabites, from the PCIGR at the University of British Columbia, analyzed sulfide, feldspar, and calcite mineral separates for Pb isotope values. Jim Mortensen and Greg Dipple are thanked for their advice regarding the interpretation of Pb isotope and C/O isotope data, respectively. Thomas Bissig, Steffen Hagemann, Steve Kesler, David Love, W.J. McMillan, and Larry Meinert are thanked for their careful reviews of the manuscript and helpful comments. The first author acknowledges financial support from the second stage of the Brain Korea 21 project at Pukyong National University. The Radiogenic Isotope Facility at the University of Alberta is supported, in part, by an NSERC Major Resources Support Grant.

Appendix 1

Whole-rock and trace element data for representative rock types in the Toodoggone district.

Appendix 2

Summary of microthermometric data from low-sulfidation epithermal Au–Ag veins in the Toodoggone district.

Appendix 3

Sulfur isotope analyses of sulfides from porphyry and epithermal occurrences in the Toodoggone district.

Appendix 4

Carbon and oxygen isotope data for calcite from porphyry and epithermal occurrences in the Toodoggone district.

Appendix 5

Lead isotope values for sulfides, feldspars, and calcite from veins and rock types proximal to porphyry and epithermal occurrences in the Toodoggone district.

References

Al-Aasm IS, Taylor BE, South B (1990) Stable isotope analysis of multiple carbonate samples using selective acid extraction. Chemical Geology: Isotope Geoscience Section 80:119–125

Arribas A Jr., Hedenquist JW, Itaya T, Okada T, Concepcion RA, Garcia JS Jr. (1995) Contemporaneous formation of adjacent porphyry and epithermal Cu–Au deposits over 300 ka in northern Luzon, Philippines. Geology 23:337–340

Bodnar RJ (1994) Synthetic fluid inclusions. XII: The system H_2O–NaCl. Experimental determination of the halite liquidus and isochores for a 40 wt% NaCl solution. Geochimica et Cosmochimica Acta 58:1053–1063

Clark JR, Williams-Jones AE (1986) Geology and genesis of epithermal gold–barite mineralization, Verrenass deposit, Toodoggone district, British Columbia. Geological Association of Canada and Mineralogical Association of Canada Annual Meeting, 57

Clark JR, Williams-Jones AE (1989) New K–Ar isotopic ages of epithermal alteration from the Toodoggone River area, British Columbia (94E). British Columbia Ministry of Energy, Mines and Petroleum Resources, Geological Fieldwork 1988, Paper 1989-1: 409–412

Clark JR, Williams-Jones AE (1991) $^{40}Ar/^{39}Ar$ ages of epithermal alteration and volcanic rocks in the Toodoggone Au–Ag district, north-central British Columbia (94E). British Columbia Ministry Energy, Mines and Petroleum Research, Geological Fieldwork 1990, Paper 1991-1: 207–216

Claveria RJR (2001) Mineral paragenesis of the Lepanto copper and gold and the Victoria gold deposits, Mankayan mineral district, Philippines. Resource Geology 51:97–106

Claypool GE, Holser WT, Kaplan IR, Sakai H, Zak I (1980) The age curves of sulfur and oxygen isotopes in marine sulfate and their mutual interpretation. Chemical Geology 28:199–260

Cooke DR, Bloom MS (1990) Epithermal and subjacent porphyry mineralization, Acupan, Baguio District, Philippines; a fluid-inclusion and paragenetic study. Journal of Geochemical Exploration 35:297–340

Coplen TB, Kendall C, Hopple J (1983) Comparison of stable isotope reference samples. Nature 302:236–238

De la Roche H, Leterrier J, Grandclaude P, Marchal M (1980) A classification of volcanic and plutonic rocks using R1 R2-diagram and major-element analyses; its relationships with current nomenclature. Chemical Geology 29:183–210

Diakow LJ (2001) Geology of the southern Toodoggone River and northern McConnell Creek map areas, north-central British Columbia. British Columbia Ministry of Energy, Mines and Petroleum Resources, Open file map 2001-1, 1:50 000 scale

Diakow LJ (2004) Geology of the Samuel Black Range between the Finlay river and Toodoggone river, Toodoggone river map area,

north-central British Columbia (parts of NTS 94E/2,6 and 7). British Columbia Ministry of Energy, Mines and Petroleum Resources, Open file map 2004-4, 1:50 000 scale

Diakow LJ (2006a) Geology between the Finlay River and Chukachida Lake, central Toodoggone River map area, north-central British Columbia (parts of NTS 94E/2, 6, 7, 10 and 11). British Columbia Ministry of Energy, Mines and Petroleum Resources, Open file map 2006-4, 1:50 000 scale

Diakow LJ (2006b) Toodoggone's Au–Cu setting unraveled. Mineral Exploration Roundup 06, Westin Bayshore, Vancouver, British Columbia, 14–15

Diakow LJ, Panteleyev A, Schroeter TG (1991) Jurassic epithermal prospects in the Toodoggone river area, northern British Columbia: examples of well preserved, volcanic-hosted, precious metal mineralization. Economic Geology 86:529–554

Diakow LJ, Panteleyev A, Schroeter TG (1993) Geology of the Early Jurassic Toodoggone Formation and gold–silver deposits in the Toodoggone river map area, northern British Columbia. British Columbia Ministry of Energy, Mines and Petroleum Resources, 72 pp

Diakow LJ, Nixon GT, Rhodes R, Lane B (2005) Geology between the Finlay and Toodoggone rivers, Toodoggone river map area, north-central British Columbia (parts of NTS 94E/2, 6 and 7). British Columbia Ministry of Energy, Mines and Petroleum Resources, Open file map 2005-3, 1:50 000 scale

Diakow LJ, Nixon GT, Rhodes R, van Bui P (2006) Geology of the central Toodoggone River map area, north-central British Columbia (parts of NTS 94E/2, 6, 7, 10 and 11). British Columbia Ministry of Energy, Mines and Petroleum Resources, Open file map 2006-6, 1:50 000 scale

Dickinson JM (2006) Jura-triassic magmatism and porphyry Au–Cu mineralization at the Pine deposit, Toodoggone district, north-central British Columbia. M.Sc. thesis, University of British Columbia, Vancouver, 116 pp

Drummond SE, Ohmoto H (1985) Chemical evolution and mineral deposition in boiling hydrothermal systems. Economic Geology 80:126–147

Duuring P, Rowins SM, McKinley BSM, Dickinson JM, Diakow LJ, Kim Y-S, Creaser RA (2008) Magmatic and structural controls on porphyry-style Cu–Au–Mo mineralization at Kemess South, Toodoggone district of British Columbia, Canada. Mineralium Deposita (this volume)

Gustafson LB, Hunt JP (1975) The porphyry copper deposit at El Salvador, Chile. Economic Geology 70:857–912

Hagemann SG, Brown PE (1996) Geobarometry in Archean lode-gold deposits. European Journal of Mineralogy 8:937–960

Hayba DO (1997) Environment of ore deposition in the Creede mining district, San Juan Mountains, Colorado: Part V. Epithermal mineralization from mixing in the OH vein. Economic Geology 92:29–44

Hedenquist JW, Arribas A Jr., Reynolds TJ (1998) Evolution of an intrusion-centered hydrothermal system; Far Southeast-Lepanto porphyry and epithermal Cu–Au deposits, Philippines. Economic Geology 93:373–404

Hedenquist JW, Henley RW (1985) The importance of CO_2 on freezing point measurements of fluid inclusions: evidence from active systems and implications for epithermal ore depositions. Economic Geology 80:1379–1406

Maniar PD, Piccoli PM (1989) Tectonic discrimination of granitoids. Geological Society of America Bulletin 101:635–643

Marsden H, Moore JM (1990) Stratigraphic and structural setting of the Shasta Ag–Au deposit (94E). British Columbia Ministry Energy, Mines Petroleum Research, Geological Fieldwork 1989, Paper 1990-1:305–314

McKibben MA, Eldridge CS (1990) Radical sulfur isotope zonation of pyrite accompanying boiling and epithermal gold deposition; a SHRIMP study of the Valles Caldera, New Mexico. Economic Geology 85:1917–1925

McKinley BSM (2006) Geological characteristics and genesis of the Kemess North porphyry Au–Cu–Mo deposit, Toodoggone district, north-central British Columbia, Canada. M.Sc. thesis, University of British Columbia, Vancouver, British Columbia, Canada, 136 pp

Monger J, Church B (1977) Revised stratigraphy of the Takla Group, north-central British Columbia. Canadian Journal of Earth Sciences 14:318–326

Mortensen JK, Ghosh DK, Ferri F (1995) U–Pb geochronology of intrusive rocks associated with copper–gold porphyry deposits in the Canadian Cordillera. In: Schroeter TG (ed) Porphyry deposits of the northwestern Cordillera of North America. Canadian Institute of Mining and Metallurgy, Montreal, pp 142–160

Ohmoto H (1986) Stable isotope geochemistry of ore deposits. In: Valley JW, Taylor HP, O'Neil JR (eds) Stable isotopes in high temperature geological processes. Mineralogical Society of America, Washington, DC, 16:491–559

Ohmoto H, Rye RO (1979) Isotopes of sulfur and carbon. In: Barnes HL (ed) Geochemistry of hydrothermal ore deposits. 2nd edn. Wiley, New York, pp 509–567

O'Neil JR, Clayton RN, Mayeda TK (1969) Oxygen isotope fractionation in divalent metal carbonates. The Journal of Chemical Physics 51:5547–5558

Pearce JA, Harris NBW, Tindle AG (1984) Trace element discrimination diagrams for the tectonic interpretation of granitic rocks. Journal of Petrology 25:956–983

Peccerillo A, Taylor SR (1976) Geochemistry of Eocene calc-alkaline volcanic rocks from the Kastamonu area, northern Turkey. Contributions to Mineralogy and Petrology 58:63–81

Peter J (1983) Mineralogy, wall rock alteration, and geochemistry of the Baker Ag–Au mine, Toodoggone River area, north-central B.C. B. Sc. thesis, University of British Columbia, Vancouver, pp 98

Rebagliati CM, Bowen BK, Copeland DJ, Niosi DWA (1995) Kemess South and Kemess North porphyry gold–copper deposits, northern British Columbia. In: Schroeter TG (ed) Porphyry deposits of the northwestern Cordillera of North America. Canadian Institute of Mining and Metallurgy, Montreal, pp 377–396

Riedel W (1929) Zur Mechanik geologischer Brucherscheinungen. Zentralblatt für Mineralogie, Geologie und Palaontologie 1929B:354–368

Roddick JC (1987) Generalized numerical error analysis with applications to geochronology and thermodynamics. Geochimica et Cosmochimica Acta 51:2129–2135

Roedder E, Bodnar RJ (1980) Geologic pressure determinations from fluid inclusion studies. Annual Review of Earth and Planetary Sciences 8:263–301

Rollinson HR (1993) Using geochemical data: evaluation, presentation, interpretation. Longman, Harlow, p 352

Rye RO (1993) The evolution of magmatic fluids in the epithermal environment; the stable isotope perspective. Economic Geology 88:733–752

Rye RO, Bethke PM, Wasserman MD (1992) The stable isotope geochemistry of acid sulfate alteration. Economic Geology 87:225–262

Sajona FG, Izawa E, Motomura Y, Imai A, Sakakibara H, Watanabe K (2002) Victoria carbonate-base metal gold deposit and its significance in the Mankayan mineral district, Luzon, Philippines. Resource Geology 52:315–328

Sawkins FJ (1990) Metal deposits in relation to plate tectonics. Springer, Berlin, p 461

Schroeter TG (1982) Toodoggone River Area (94E). B.C. Ministry of Energy, Mines and Petroleum Resources, Geological Fieldwork 1981, Paper 1982-1:122–133

Sharp Z (2006) Principles of stable isotope geochemistry. Pearson Prentice Hall, Upper Saddle River, p 344

Shepherd TJ, Rankin AH, Alderton DHM (1985) A practical guide to fluid inclusion studies. Blackie, Glasgow, p 239

Sillitoe RH, Hedenquist JW (2003) Linkages between volcanotectonic settings, ore–fluid compositions, and epithermal precious metal deposits. Special Publication for the Society of Economic Geologists 10:315–343

Simmons HW, Browne PRL (2000) Hydrothermal minerals and precious metals in the Broadlands–Ohaaki geothermal system: implications for understanding low-sulfidation epithermal environments. Economic Geology 95:971–999

Simmons SF, White NC, John DA (2005) Geological characteristics of epithermal precious and base metal deposits. Economic Geology 100th Anniversary Volume:485–522

Taylor BE (1987) Stable isotope geochemistry of ore-forming fluids. In: Kyser TK (ed) Short Course Handbook. 13:337–445

Thiersch PC, Williams-Jones AE, Clark JR (1997) Epithermal mineralization and ore controls of the Shasta Au–Ag deposit, Toodoggone District, British Columbia, Canada. Mineralium Deposita 32:44–57

Thirlwall MF (2000) Inter-laboratory and other errors in Pb isotope analyses investigated using a ^{207}Pb–^{204}Pb double spike. Chemical Geology 163:299–322

Veizer J, Ala D, Azmy K, Bruckschen P, Buhl D, Bruhn F, Carden GAF, Diener A, Ebneth S, Godderis Y, Jasper T, Korte C, Pawellek F, Podlaha OG, Strauss H (1999) $^{87}Sr/^{86}Sr$, $\delta^{13}C$ and $\delta^{18}O$ evolution of Phanerozoic seawater. Chemical Geology 161:59–88

Winchester JA, Floyd PA (1977) Geochemical discrimination of different magma series and their differentiation products using immobile elements. Chemical Geology 20:325–343

Zartman RE, Doe BR (1981) Plumbotectonics; the model. Tectonophysics 75:135–162